ENGINEERING RESEARCH INSTITUTE
THE UNIVERSITY OF MICHIGAN
ANN ARBOR

Final Report

AN INVESTIGATION OF INTERGRANULAR OXIDATION IN STAINLESS STEELS AND HIGH-NICKEL ALLOYS

WADC Technical Report 55-470 Part 2

Clarence A. Siebert
Maurice J. Sinnott
Lynn H. DeSmyter
Harry M. Ferrari

Materials Laboratory

Project 2110

UNITED STATES AIR FORCE
WRIGHT AIR DEVELOPMENT CENTER
AIR RESEARCH AND DEVELOPMENT COMMAND
WRIGHT-PATTERSON AIR FORCE BASE, OHIO
CONTRACT NO. AF 33(616)-353, PROJECT NO. 54-670-60

July 1956

FOREWORD

This report was prepared by The University of Michigan, under USAF Contract No. AF 33(616)-353. The contract was initiated under Project No. 54-670-60, and was administered under the direction of the Materials Laboratory, Directorate of Research, Wright Air Development Center, with Lt Richard Agricola acting as project engineer.

ABSTRACT

Specimens from Chromel ASM, Hastelloy B, and commercial and vacuum-melted type 310 alloys were oxidized for 100-hour periods in the stressed condition. Intergranular oxidation measurements were obtained microscopically. In general, the intergranular penetrations increased rapidly with stress after a certain minimum value was reached. This minimum value, denoted as the threshold stress, was determined for each alloy at various temperatures. The weight gained during oxidation was determined. It was found that most of the alloys tested followed the parabolic oxidation law.

PUBLICATION REVIEW

This report has been reviewed and is approved.

FOR THE COMMANDER:

M. R. WHITMORE
Technical Director
Materials Laboratory
Directorate of Research

TABLE OF CONTENTS

LIST OF TABLES

LIST OF FIGURES

LIST OF FIGURES
(Continued)

LIST OF FIGURES
(Continued)

LIST OF FIGURES
(Continued)

LIST OF FIGURES
(Concluded)

INTRODUCTION

When a metal is subjected to an oxidizing medium the usual result is the formation of a continuous oxide layer on the exposed surface. In general, the oxide layer increases in thickness with increasing time and/or temperature of exposure. With some alloys, however, oxidation also occurs in the grain boundaries ahead of the metal-oxide interface. This report is primarily concerned with this grain-boundary oxidation, although the volume or lattice oxidation rate will affect the measured grain boundary and, therefore, must be considered as well.

Intergranular oxidation becomes an important factor in applications where thin sections are exposed to air at high temperatures. Under these conditions, the portion of the metal influenced by these oxide fissures is a significant percentage of the whole and may result in premature failure.

The present program arose from the need of the U. S. Air Force for information concerning intergranular oxidation in stainless steels and high-nickel alloys at high temperatures. There were three objectives in this research program:

1. to investigate the effect of temperature and stress on the progressive intergranular oxidation and to determine the threshold stress of some stainless steels and high-nickel alloys at temperatures of 1200°F and above,
2. to measure the oxidation rates of these materials by means of the weight gained during oxidation, and
3. to study the subsurface oxides.

EQUIPMENT

The equipment used during this investigation was the stress-oxidation and continuous weight-gain apparatus described in WADC TR 55-470 Pt 1. Another stress-oxidation unit similar to those described in the above report was constructed.

PROCEDURE

Specimen Preparation

The specimens for the stressed-oxidation tests were prepared as standard strip specimens having a 1/2 x 2-inch gauge portion. A detailed description of the specimen was given in the previous report (1).

The specimens for the weight-gain measurements were 2 x 1-inch rectangles of the as-received material containing a 1/64-inch hole near the top for the insertion of the platinum suspension wire.

Operating Procedure

The oxidation procedure for the stressed-oxidation tests was the same as that used during the previous investigation (1), except that the specimens were not quenched but air-cooled. Since x-ray analysis of the oxides was no longer a regular part of the investigation, this simplification was possible.

The weight-gain procedure was the same as that described in the previous report.

The metallographic polishing procedure also was the same as that used previously.

Evaluation of Specimens

The polished specimens were measured to determine the extent of intergranular penetration. The mean depth ($\bar{x}$) and the total number of penetrations (N) were then determined from the penetration measurements. A complete description of the method of taking and evaluating penetration data is given in WADC TR 54-120 (2).

In brief, the method consisted of examining the polished specimen at 500 diameters, using a calibrated, No. 6 grain-size eyepiece. The grid, containing 6 squares in the side, was aligned with the specimen edge, and the number of penetrations and their depths were obtained by traversing the edge over a distance of approximately 2 inches.

In addition to the procedure used in the previous years (1,2), another method of evaluating and presenting the penetration data was used. Repeated measurements on the same specimen showed that the most uncertain types of penetrations are the extremely small ones, i.e., the ones which lie in the first group. Generally these represent true intergranular penetrations, as is shown by high-magnification examination. However, some are the result of polishing artifacts or are surface-roughness effects which usually occur during oxidation.

In addition to being somewhat uncertain, these small penetrations dominate the evaluation with respect to total number and mean depth, since they are present to a greater extent than the deeper ones. To make the effect of stress and temperature on the deeper and more significant penetrations more noticeable, it was decided to make a modified number and mean-depth calculation, excluding the smaller penetrations. To do this the first group, and in a few instances the first and second groups, was excluded and a modified number and mean-depth calculation made. This new method shows the changes in the penetration character in the critical regions to a more marked extent.

Metallographic Studies

In conjunction with the penetration studies described above, each specimen was carefully examined metallographically, using the optical microscope. The specimens which exhibited the phenomenon called "fissuring" were classified according to the degree to which this fissuring was observed. Figures 1 through 8 were given the arbitrary designations one through eight, from smaller to greater fissuring, and were used to give a numerical value to the extent of fissuring on all samples that exhibited the phenomenon. The numeral "zero" was used to designate specimens which exhibited no fissuring.

The specimens were also examined for any changes in microstructure which might occur during testing.

MATERIAL

The materials used in this investigation consisted of specimens from Chromel ASM alloy, heat 25139 of commercial type 310 alloy, heat B-1400 of Hastelloy B, and heat 4X-343 of vacuum-melted type 310 alloy. The type 310 stainless alloys and the Chromel ASM alloy were received in the form of cold-rolled and annealed strip 1.0 x 0.5 inch, and the Hastelloy B in the form of hot-rolled strip 1.0 x 0.38 inch, which had received a light cold-roll pass to improve the surface, and a final anneal. The chemical analyses of the heats are presented in Table I.

RESULTS AND DISCUSSION

For purposes of discussion this section has been divided into three parts, namely: (1) weight-gain investigation, (2) stress-oxidation investigation, and (3) metallographic investigation.

Weight-Gain Investigation

A visual study of the depth of intergranular oxidation at high temperatures is of limited value by itself. Some knowledge of the volume of oxidation should also be known before an alloy can be properly evaluated, since an apparently low rate of intergranular penetration may result from a high-volume oxidation. A continuous weight-gained measuring apparatus has been used for measuring oxidation rates. It should be noted that the weight gained during oxidation is a measure of both the lattice and the intergranular oxidation; however, the intergranular oxidation probably is a small contributing factor compared to the lattice oxidation.

The experimental data, when plotted as square of the weight gained vs time, are linear, as shown in Figs. 9 through 12. Most samples show some deviation from the parabolic oxidation law in the early stages, as can be seen from the fact that the linear plots do not go through the origin. This initial deviation is usually found in oxidation studies, and the theoretical reasons for its occurrence have been stated by Gulbransen and Andrew (3).

Because of these deviations which occur at the initial stages of testing, the parabolic rate constant (slope of ΔW^2-vs-time curve) is probably a better indication of the volume oxidation than the specific weight gained after a given time. Figures 9 through 12 are plots of weight gained squared vs time for the four alloys investigated, and Table II is a summary of the parabolic weight-gained constants.

The rate constant of the Chromel ASM alloy at 1800°, 1900°, and 2000°F is lower than the rate constants of any of the other alloys investigated.

The Hastelloy B has a much greater rate of oxidation than the other alloys investigated, and at 1600° and 1800°F the rate constant is 0.047 and 0.36, respectively, the latter being almost tenfold greater than any value obtained on any of the other alloys tested. This factor, combined with the fact that the oxide layer flakes off during cooling, would limit the use of this material in this temperature range.

Stress-Oxidation Investigations

Several alloys have been investigated at varying stresses and temperatures for the determination of their intergranular oxidation characteristics under stress. The stress levels were chosen so as to give a representative count of intergranular penetration in the low stress regions and were concentrated in the region where the stress caused an increase in the intergranular penetration. The object was to locate the test points near, but not in, the region where fissuring throughout occurred, i.e., fissuring to the extent shown in Figs. 5 through 8. Since each material has its own characteristic attributes, the alloys will be considered individually.

Chromel ASM

The Chromel ASM alloy was tested at various stress levels at temperatures of 1700°, 1800°, 1900°, and 2000°F. This alloy proved to be difficult to evaluate because of a large number of small penetrations and because of a precipitate throughout the matrix which at times appeared to be intergranular penetration. The great number of shallow entries is thought to be the result of a surface skin of fine grains present in the as-received material, as shown in Fig. 55. This alloy had approximately double the total number of penetrations of any other alloy tested.

The variation in the number of intergranular penetrations with depth below the metal interface at constant temperature is given in Figs. 13 through 16. These curves follow the general decay-type curve as described in WADC TR 54-120.

Figures 17 through 24 show the variation in mean depth ($\bar{x}$) and number (N) of intergranular penetrations with stress at temperatures of 1700°, 1800°, 1900°, and 2000°F. The number of penetrations is the total number counted per inch, and the mean depth is an average depth of penetration. These parameters are discussed in detail in WADC TR 54-120. In addition, as described in the procedure section of this report, another method of presenting the data was used. Modified number and mean-depth curves excluding all the small penetrations which fall in the first group, and in some instances excluding the first and second groups, are presented in some of the graphs. As can be seen in Figs. 19 through 24 these modified curves tend to follow the elongation curve more closely and exhibit a more marked change in penetration characteristics as the threshold stress is approached. The elongation curves, which are plotted on these graphs, represent the permanent elongation, as measured at room temperature after the stress had been relieved. Because all the penetrations shallower than the first group (0.00059 inch) are placed in the same class, there exists a minimum value of mean depth which can be obtained. This value is shown as a dotted line on some of the mean-depth graphs.

Figures 17 and 19, illustrating the variation in penetration number with stress at temperatures of 1700° and 1800°F, show an initial increase in number, followed by a decrease in number, as the stress is increased. At 1900° and 2000°F the number increases with no increasing stress as shown in Figs. 21 and 23. No explanation for the above behavior can be offered at this time. When the small penetrations are eliminated, the number of penetrations increases slowly at first as the stress is increased, and then increases abruptly as the threshold stress is reached at 1800°, 1900°, and 2000°F. These modified curves tend to follow the elongation curves and appear to be more significant than the regular curves.

Figures 18, 20, 22, and 24, illustrating the effect of stress on the mean depth at constant temperature, show a more or less constant mean depth with increasing stress, until a critical region is reached where the mean depth increases. The extent of this increase is a function of the testing temperature.

Figures 18 and 20 show that the mean depth of penetration is but little affected by stress in the 1700° and 1800°F samples. The 1900° and, to a greater extent, the 2000°F specimens, however, reveal in Figs. 22 and 24 that a significant increase in the mean depth occurs when this critical stress level is reached. The modified curves appear to show a constant mean depth as stress increases until the threshold stress is reached, then the mean depth increases very sharply.

The elongation of the specimen seems to have a profound effect on the intergranular penetration. In the 1700° and 1800°F tests the elongation reaches a value of only 2-5% when the material begins to fissure throughout. However, in the 1900° and 2000°F specimens the fissuring throughout did not occur until the elongation had reached a value of approximately 8% in the 1900°F specimens and 30% in the 2000°F specimens. Since these latter temperatures were the ones which showed the greatest increase in penetration, it is possible that the elongation itself is a major factor, or that it is but a measure of the intensity of circumstances which cause this increase in penetration depth.

As outlined in the introduction, one of the objects of this investigation is to determine the threshold stress, i.e., the stress at a given temperature where a material begins to exhibit a sharp increase in intergranular penetration. For the Chromel ASM alloy this stress corresponds very closely to the stress at which the elongation greatly increases. This can be seen in Figs. 17 through 24 as a large change in slope in the elongation-vs-stress curve. Of course, the value of this threshold stress is somewhat arbitrary and is a function of what is considered to be a significant increase. In this case the beginning of the sharp increase in penetration depth was considered to be the threshold stress. For the Chromel ASM alloy these stresses were found to be 2000, 1400, 900, and 600 psi at temperatures of 1700°, 1800°, 1900°, and 2000°F, respectively.

The data obtained from the stress investigation for the Chromel ASM alloy are summarized in Table III.

Commercial Type 310 Alloy, Heat 25139

The variation in the number of intergranular penetrations with depth below the oxide surface at constant testing temperatures is given in Figs. 25 through 28. These curves follow the general decay type as described in WADC TR 54-120. As the temperature of testing is increased, the number of deep penetrations increases. When the stress at a given temperature is increased, the number of deep penetrations also increases.

Figures 29 through 36 are the penetration-number and mean-penetrations-depth graphs. The elongation is plotted for all samples tested in both types of graphs, although it was impossible to obtain penetration data on some of the more highly stressed samples since they contained fissures throughout the matrix. In the 1700°, 1800°, and 2000°F tests the number decreases as the stress is increased when all groups are considered. However, the number of

deep penetrations is increased when the minor groups are excluded. In Fig. 29 (1700°F) the curve excluding the first group showed an increase in penetration number with increasing stress, while the 1800° and 2000°F graphs showed a decrease even when the first group was excluded, as shown in Figs. 31 and 35. Excluding the first and second groups showed no appreciable effect of stress on number in the 1800° and 2000°F graphs. Figure 33 (1900°F) shows an increase in the number of penetrations for the total number as well as for the condition when the minor groups are excluded.

Figures 30 and 34 show that the mean depth considering all penetrations, increases significantly in the 1700° and 1900°F tests, and this is noticeable when the first group is omitted. The 1800°F graph shows a shift in the shape of the curve as the number of groups considered is decreased. Considering all groups, the mean depth decreases slightly, while excluding the first group shows no effect of stress, and excluding the first and second groups shows a significant increase in the mean depth.

It was estimated that the threshold stresses occur at 2300, 1400, 900, and 600 psi at temperatures of 1700°, 1800°, 1900°, and 2000°F.

The data obtained from the stress investigation for commercial 310 alloy are summarized in Table IV.

Hastelloy B, Heat B-1400

The Hastelloy B material was tested at temperatures of 1200°, 1400°, 1600°, and 1800°F in the stress-oxidation units. Figures 37 through 40 are the penetration-frequency graphs giving the relationship between penetration depth and number. These curves are of the decay-curve type previously discussed. The effect of stress in the critical region (that region where the material elongates considerably) could not be determined for the 1200°F tests since the units were not constructed to carry a load greater than 200 lb. A 1/4-inch-wide section was the smallest practical specimen size, and therefore the maximum stress obtainable to produce much elongation was about 20,000 psi, which was insufficient. The testing at 1200°F was therefore discontinued when 20,000 psi showed negligible elongation at the end of the test.

Figures 41 through 48 show the effect of stress on the number and mean depth of penetrations. The 1200°F tests were conducted at a stress below the critical range, as previously discussed, and therefore do not show any appreciable effect. Since all the penetrations encountered were extremely small, the slight increase in number is not considered significant. The large amount of scatter encountered in the 1400°F curve makes the effect of stress on number difficult to determine, while the 1600°F shows an increase and the 1800°F a slight decrease in number. Excluding the first group shows an increase in the number of deep penetrations in the 1800°F graph. This exclusion is of no value in the lower-temperature tests since the penetrations are for the most part in the first group. The mean depth of penetration is not appreciably affected by

stress in the 1200°, 1400°, and 1600°F tests as shown in Figs. 42, 44, and 46. In the 1800°F tests, however, the mean depth is increased significantly with increasing stress. This is especially noticeable in the deeper penetrations, as is shown by the curves excluding the minor groups. It was not possible to obtain a great deal of elongation in the 1800°F tests. Some specimens, which fractured during the latter part of the test, showed only 3.5% elongation.

The threshold stresses were estimated as occurring at stresses of 15000, 6000, and 3500 psi for temperatures of 1400°, 1600°, and 1800°F, respectively. This latter value at 1800°F is more than twice as great as values obtained for either Chromel ASM or the type 310 alloys for the same temperature.

The data obtained from the stress investigation for the Hastelloy B are summarized in Table V.

Vacuum-Melted Type 310 Alloy, Heat 4X-343

This alloy was tested only at 1900° and 2000°F because of limited time. Figures 49 and 50 show the penetrations-vs-depth curves at various stress levels. Again, the curves are of the decay type.

Figures 51 through 54 show the effect of stress on the number and mean depth of penetrations. The number of penetrations appears to be independent of the stress at both 1900° and 2000°F when all groups are considered. At 1900°F, when the first group is excluded, the number still remains approximately constant, but excluding both the first and second groups shows an increase in number with increasing stress at 2000°F.

The mean depth at 1900°F remains approximately constant as a function of stress when all groups are considered, and also when the minor groups are excluded. At 2000°F the mean depth remains fairly constant at first, and then increases as the critical region is reached. The reason why the mean depth at 1900°F does not show an increase is that the critical region has not quite been reached, as can be seen from the fact that at the highest stress tested the sample just barely showed enough fissures to be classified in fissuring class No. 1. Apparently at this temperature the elongation increases considerably before the alloy exhibits any fissuring.

Approximate values for the threshold stresses in this alloy are 900 and 650 psi at temperatures of 1900° and 2000°F, respectively. This vacuum-melted alloy has intergranular penetration characteristics which are comparable to that of the commercial type 310 alloy.

The data obtained from the stress investigation for the vacuum-melted 310 alloy are summarized in Table VI.

Metallographic Examination

Photomicrographs of each of the four alloys in the as-received condition are presented in Figs. 55 through 58. These phogomicrographs were taken to provide a standard of reference for photomicrographs taken following testing.

Figure 55 illustrates the surface layer of small grains which is present in the as-received Chromel ASM alloy. The commercial type 310 alloy has a twinned, medium-sized grain structure. Examination at 1000x shows the presence of a discontinuous grain-boundary carbide network. The Hastelloy B material in the as-received condition has a banded structure of two rows of large grains at the center with fine grains on either side of the bands, as shown in Fig. 57. The as-received vacuum-melted type 310 alloy has a grain structure similar to that of the commercial 310 alloy, except that examinination at 1000x shows a more continuous carbide network in the grain boundaries.

After testing, the Chromel ASM alloy still exhibits the fine-grained surface layer. Considerable grain growth occurs at 2000°F, as can be seen by comparing Fig. 69 with 55; however, the surface layer still remains much finer than the matrix.

Type 310 alloy, heat 25139, exhibits no grain growth at 1700° and 1800°F, but does exhibit appreciable grain growth at 1900° and 2000°F, as can be seen by comparing Figs. 59 through 62 with Fig. 56. The final grain size at any given temperature is practically independent of the applied stress. The final structure after testing is generally quite similar to that in the as-received condition. The appearance of a new phase is detected only when stresses sufficiently high to cause much "fissuring" are used. At these high stresses, the appearance of an excess phase, as shown in Fig. 70, occurs. Microhardness impressions indicate that the excess phase is much harder than the matrix. Although it has not been positively established, it is thought that this phase is a high nitrogen-chromium compound. A similar phase found in creep-rupture specimens of 18-8 stainless steel was identified as a high nitrogen phase by Smith (4).

The banded structure of the Hastelloy B material in the as-received condition appears to be minimized after heating for 100 hours at the testing temperatures, as shown in Figs. 63 through 66.

The vacuum-melted type 310 alloy exhibits very little grain growth at 1900° and 2000°F (Figs. 67 and 68) compared to the as-received condition (Fig. 58). No phase changes were detected during testing in this vacuum-melted alloy; however, it is possible that an excess phase similar to that shown in Fig. 70 for the commercial 310 alloy might occur if sufficiently high stresses were used to cause "fissuring."

SUMMARY AND CONCLUSIONS

1. The weight gained at various time intervals during oxidation was determined for Chromel ASM, Hastelloy B, and commercial and vacuum-melted type 310 alloys at temperatures varying from 1200° to 2000°F. Most of the alloys tested followed the parabolic oxidation law. The parabolic rate constant was determined for each specimen investigated.

2. The Chromel ASM alloy had the lowest and the Hastelloy B the highest parabolic rate constants of the alloys tested. The commercial and the vacuum-melted 310 alloys had approximately the same parabolic rate constants.

3. Chromel ASM, Hastelloy B, and commercial and vacuum-melted type 310 alloys were oxidized at various stress levels for 100-hour periods at temperatures ranging from 1200° to 2000°F. Intergranular penetration measurements were made and the data presented as follows: (1) penetration frequency vs depth, (2) penetration number (N) vs stress, and (3) the mean depth ($\bar{x}$) vs stress.

4. The threshold stress, i.e., the stress at which a sharp increase in depth of intergranular penetrations occurs, was determined for each alloy at various temperatures. At 1900° and 2000°F, the threshold stress occurred at approximately the same value for the Chromel ASM alloy, commercial type 310 alloy, and the vacuum-melted 310 alloy.

BIBLIOGRAPHY

1. Siebert, C. A., Sinnott, M. J., Keith, R. E., and DeSmyter, L. H., An Investigation of Intergranular Oxidation in Stainless Steels and High-Nickel Alloys, WADC TR 55-470 Pt 1, April, 1955.

2. Siebert, C. A., Sinnott, M. J., and Keith, R. E., An Investigation of Intergranular Oxidation in Stainless Steels, WADC TR 54-120, January, 1954.

3. Gulbransen, E. A., and Andrew, K. F., J. Electrochem. Soc., 98, 241 (1951).

4. Smith, G. V., Dulis, E. J., and Houston, G. E., Trans. ASM, 42, 935 (1950).

TABLE I

CHEMICAL ANALYSIS OF MATERIALS, WEIGHT PERCENT

Alloy and Heat No.	Fe	Ni	Cr	Mn	Si	C	S	P	Co	Mo	V
Chromel, ASM	0.37	77.65	19.81	0.30	1.43	0.05	-----	-----	----	-----	----
Type 310, 25139	Bal	19.26	25.42	1.58	0.62	0.05	-----	-----	----	-----	----
Hastelloy B	5.19	-----	0.26	0.60	0.24	0.03	-----	-----	0.74	28.01	0.45
Type 310, 4X-343*	Bal	20.35	25.14	1.87	0.63	0.147	0.029	0.021	----	-----	----

*Vacuum-melted heat.

TABLE II

PARABOLIC RATE CONSTANT OBTAINED FROM WEIGHT-GAIN OXIDATION STUDIES IN $(mg/in.^2)(1/min)$

Oxidizing Temperature (°F)	Chromel ASM	Type 310 Alloy Heat 25139	Hastelloy B Heat B-1400	Type 310 Alloy Heat 4X-343
1200			0.0012	
1400			0.025	
1600			0.047	
1700		0.0027		
1800	0.000133	0.0053	0.36	
1900	0.0005	0.017		0.019
2000	0.00183	0.043		0.045

TABLE III

RESULTS OF STRESS-OXIDATION ON CHROMEL ASM ALLOY

Temp. (°F)	Stress psi	Elong. %	Including All Groups		Excluding Group I		Excluding Groups I and II		Fissuring Class Number
			N	$\bar{x} \times 10^3$	N	$\bar{x} \times 10^3$	N	$\bar{x} \times 10^2$	
1700	----	----	1645	0.301	2	0.880	-----	-----	0*
	1150	0	3164	0.306	31	0.880	-----	-----	0
	1535	0	3299	0.302	14	0.880	-----	-----	0
	2000	0.5	2034	0.317	59	0.886	0.6	1.480	0
	2100	1.0	3019	0.304	23	0.880	-----	-----	0
	2150	1.5	3363	0.358	23	0.880	-----	-----	0
	2200	2.5	2712	0.303	16	0.880	-----	-----	0
	2210	12.0	Fiss	Fiss	---	-----	-----	-----	5
	2240	6.5	Fiss	Fiss	---	-----	-----	-----	5
	2250	24.0	Fiss	Fiss	---	-----	-----	-----	8
	2490	22.5	Fiss	Fiss	---	-----	-----	-----	7
	2880	16.0	Rupt	Rupt	---	-----	-----	-----	7
1800	0	----	2957	0.311	55	0.880	-----	-----	0
	405	0	1876	0.306	18	0.880	-----	-----	0
	960	0	3279	0.313	72	0.897	2	1.480	0
	1250	1.5	2278	0.300	1	0.880	-----	-----	0
	1500	1.5	2419	0.304	15	0.880	-----	-----	0
	1520	3.5	3012	0.361	176	0.944	15	1.636	0
	1550	5.5	2736	0.375	228	0.908	9.8	1.527	0
	1560	4.5	2861	0.319	93	0.898	2.4	1.577	0
	1600	18.0	Fiss	Fiss	---	-----	-----	-----	5-6
	1600	15.0	Fiss	Fiss	---	-----	-----	-----	6
	1750	19.0	Fiss	Fiss	---	-----	-----	-----	8
	2000	28	Fiss	Fiss	---	-----	-----	-----	8
1900	0	----	2634	0.344	157	0.880	-----	-----	0
	400	0	1762	0.358	173	0.887	2	1.480	0
	750	1.0	2091	0.317	63	0.880	-----	-----	0
	750	2.0	2448	0.448	586	0.917	36	1.480	0
	1000	6.0	2309	0.395	314	0.973	35	1.713	0
	1060	6.5	2438	0.406	360	1.020	64.6	1.664	0
	1075	3.0	3044	0.394	71	0.905	3	1.480	0
	1100	6.0	1407	0.455	130	0.949	13	1.569	0
	1105	8.5	2222	0.495	531	1.115	137	1.792	0
	1120	13.0	3043	0.618	737	1.445	317	2.193	2
	1125	16.5	Fiss	Fiss	---	-----	-----	-----	4-5
	1250	29.0	Fiss	Fiss	---	-----	-----	-----	8
2000	0	----	1648	0.472	271	0.913	14	1.521	0
	300	0.5	1910	0.430	369	0.960	47	1.505	0
	500	2.5	2019	0.426	401	0.937	36	1.512	0
	600	4.0	1062	0.476	225	0.999	381	1.584	0
	650	6.0	1396	0.414	251	0.934	19	1.588	0
	680	18.5	Fiss	Fiss	---	-----	-----	-----	7
	700	10.0	2518	0.657	721	1.394	276	2.222	2
	750	22.0	Fiss	Fiss	---	-----	-----	-----	7
	750	34.0	Fiss	Fiss	---	-----	-----	-----	8
	750	10.0	2751	0.571	627	1.334	233	2.101	1
	805	31.0	Fiss	Fiss	---	-----	-----	-----	8
	1000	55.0	Fiss	Fiss	---	-----	-----	-----	8

* 0 designates no fissuring.

TABLE IV

RESULTS OF STRESS-OXIDATION ON TYPE 310 ALLOY, HEAT 25139

Temp. (°F)	Stress psi	Elong. %	Including All Groups		Excluding Group I		Excluding Groups I and II		Fissuring Class Number
			N	$\bar{x} \times 10^3$	N	$\bar{x} \times 10^3$	N	$\bar{x} \times 10^2$	
1700	975	1.0	1912	0.351	88	0.921	6	1.480	0
	2000	1.0	1615	0.317	47	0.880	-----	-----	0
	2245	2.5	1448	0.310	25	0.880	-----	-----	0
	2350	5.0	2054	0.315	51	0.886	0.5	1.480	0
	2385	5.5	1484	0.330	76	0.880	-----	-----	0
	2420	6.0	1427	0.313	32	0.880	-----	-----	0
	2500	7.0	2468	0.391	233	0.993	36	1.609	0
	2550	6.0	1207	0.323	461	0.893	1	1.480	0
	2610	7.5	1294	0.323	45	0.957	3.5	1.885	0
	2710	12.0	1252	0.473	199	1.384	89	2.009	0
1800	750	0	1780	0.473	531	0.880	-----	-----	0
	1000	3.5	1772	0.497	601	0.880	0.5	1.480	0
	1065	3.5	1687	0.503	589	0.882	2	1.480	0
	1300	8.5	1699	0.488	546	0.884	4	1.480	0
	1395	23.5	1782	0.659	683	1.236	204	2.072	3-4
	1400	14.0	----	-----	---	-----	-----	-----	0
	1500	8.0	1428	0.465	406	1.881	1	1.480	0
	1550	6.0	1342	0.449	340	0.888	4.5	1.544	0
	1580	43.0	Fiss	Fiss	---	-----	-----	-----	7
	1580	6.0	1433	0.428	315	0.884	2	1.480	0
	1690	12.0	1196	0.441	254	0.961	22.1	1.818	2
	1800	37.0	Fiss	Fiss	---	-----	-----	-----	8
1900	395	1.5	----	-----	---	-----	-----	-----	0
	755	5.5	1622	0.454	429	0.898	13	1.480	0
	900	12.5	1872	0.490	562	0.933	42.6	1.582	0
	952	14.0	1329	0.466	346	0.917	17.5	1.613	0
	1010	15.0	1790	0.504	580	0.932	44	1.559	0
	1020	22.0	Fiss	Fiss	---	-----	-----	-----	3-4
	1050	31.0	1539	0.628	470	1.375	192	2.093	0
	1100	28.0	Fiss	Fiss	---	-----	-----	-----	7-8
	1510	28.0	Fiss	Fiss	---	-----	-----	-----	8
	2000	42.0	2225	0.922	1078	1.457	500	2.124	8
2000	300	1.5	2016	0.519	664	0.966	91	1.505	0
	500	3.5	1986	0.540	702	0.981	110	1.522	0
	570	4.0	1885	0.479	534	0.936	50	1.480	0
	600	6.0	1664	0.503	521	0.950	61	1.480	0
	620	6.0	1712	0.516	853	0.971	118	1.539	0
	650	7.0	1777	0.522	600	0.959	73.5	1.572	0
	755	8.5	1676	0.512	555	0.962	64.2	1.586	1

TABLE V

RESULTS OF STRESS-OXIDATION ON HASTELLOY B, HEAT B-1400

Temp. (°F)	Stress psi	Elong. %	Including All Groups N	Including All Groups $\bar{x} \times 10^3$	Excluding Group I N	Excluding Group I $\bar{x} \times 10^3$	Excluding Groups I and II N	Excluding Groups I and II $\bar{x} \times 10^2$	Fissuring Class Number
1200	2050	0	858	0.301	---	-----	-----	-----	0
	10250	0	975	0.302	---	-----	-----	-----	0
	15000	0	1210	0.305	---	-----	-----	-----	0
	19250	0	949	0.305	---	-----	-----	-----	0
1400	1000	0	----	-----	---	-----	-----	-----	0
	4960	0	1077	0.300	---	-----	-----	-----	0
	5140	0	1517	0.300	---	-----	-----	-----	0
	7470	0.5	969	0.300	---	-----	-----	-----	0
	7775	0.5	788	0.301	---	-----	-----	-----	0
	8180	0	1288	0.300	---	-----	-----	-----	0
	8650	0.5	945	0.301	---	-----	-----	-----	0
	8900	0.5	860	0.300	---	-----	-----	-----	0
	10000	0.5	880	0.300	---	-----	-----	-----	0
	11800	1.5	686	0.300	---	-----	-----	-----	0
	15700	2.0	1080	0.306	---	-----	-----	-----	0
	16900	1.5	693	0.303	---	-----	-----	-----	0
	17700	5.5	1348	0.308	---	-----	-----	-----	0
	19000	7.0	1546	0.312	---	-----	-----	-----	
1600	1000	0	722	0.300	---	-----	-----	-----	0
	3000	0	707	0.300	---	-----	-----	-----	0
	5380	0	784	0.300	---	-----	-----	-----	0
	6800	1.5	1243	0.311	---	-----	-----	-----	0
	7100	1.5	1044	0.300	---	-----	-----	-----	0
	7340	1	1471	0.300	---	-----	-----	-----	0
	7530	1	1132	0.301	---	-----	-----	-----	0
	7800	3.5	957	0.305	---	-----	-----	-----	0
	8230	3	952	0.375	---	-----	-----	-----	0
	8904	5	1089	0.317	---	-----	-----	-----	0
	10000	10	Fiss	Fiss	---	-----	-----	-----	4
1800	500	0	1202	0.381	168	0.880	-----	-----	0
	1500	1	1165	0.426	215	0.881	0.5	1.480	0
	3000	1	1321	0.434	298	0.895	6.2	1.611	0
	3500	1.0	1356	0.449	293	0.989	28.5	2.003	0
	3650	0.5	1295	0.408	236	0.890	4.0	1.480	0
	3800	0	1364	0.423	289	0.880	-----	-----	0
	3800	3.5	1238	0.593	429	1.145	142.7	1.677	0
	3800	1	1380	0.422	276	0.907	10.6	1.584	0
	3850	3	933	0.535	246	1.191	59.5	2.169	0
	3900	2.5	1117	0.469	309.	1.005	38.4	1.892	0
	3950	3.5	1238	0.593	311	1.166	61.1	2.336	0
	4020	3	1169	0.408	174	1.024	20.0	2.141	0
	4180	3.5	Rupt	-----	---	-----	-----	-----	4

TABLE VI

RESULTS OF STRESS-OXIDATION ON TYPE 310 ALLOY, HEAT 4X-343

Temp. (°F)	Stress psi	Elong. %	Including All Groups N	Including All Groups $\bar{x} \times 10^3$	Excluding Group I N	Excluding Group I $\bar{x} \times 10^3$	Excluding Groups I and II N	Excluding Groups I and II $\bar{x} \times 10^2$	Fissuring Class Number
1900	300	2.4	1713	0.343	127	0.882	0.5	1.480	0
	400	3.5	1672	0.343	124	0.882	0.5	1.480	0
	600	6.0	1687	0.320	58	0.880	---	-----	0
	670	9.0	1639	0.337	105	0.880	---	-----	0
	750	10.2	1740	0.347	140	0.883	0.7	1.480	0
	750	10.2	1751	0.343	129	0.880	---	-----	0
	850	15.5	1559	0.345	120	0.885	1.0	1.480	0
	900	18.5	1598	0.350	132	0.899	4.2	1.480	0
	950	14.5	1459	0.340	96	0.897	2.8	1.480	1
2000	200	1.6	1597	0.398	176	0.917	10.8	1.480	0
	300	2.4	1537	0.3605	159	0.884	1.0	1.480	0
	400	6.3	1708	0.355	161	0.882	0.5	1.480	0
	454	7.5	1518	0.337	94	0.893	2.1	1.480	0
	500	11.5	1700	0.368	193	0.901	6.8	1.480	0
	600	----	1657	0.406	210	0.933	17.4	1.497	0
	650	13.0	1709	0.362	176	0.905	7.4	1.480	0
	689	15.5	1557	0.404	255	0.936	18.5	1.665	0
	720	12.0	1675	0.382	219	0.925	15.2	1.526	1
	750	23.2	1501	0.389	183	1.027	25.5	1.937	1

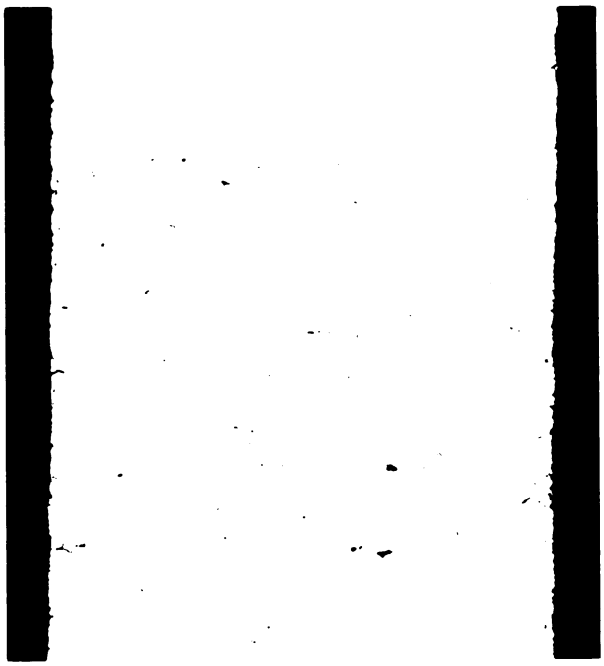

Fig. 1. Slight fissuring in matrix, Chromel ASM alloy, 2000°F, 100 hr, stress 750 psi, 50x, cross section, unetched.

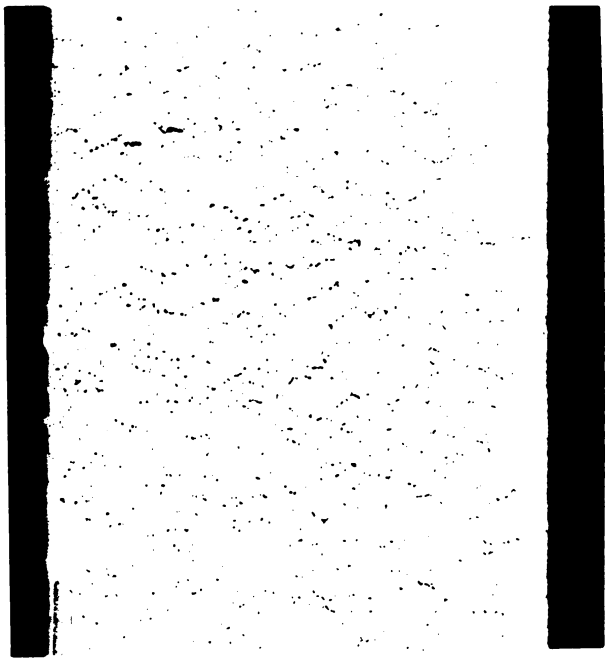

Fig. 2. Slight fissuring in matrix, Chromel ASM alloy, 1900°F, 100 hr, stress 1120 psi, 50x, cross section, unetched.

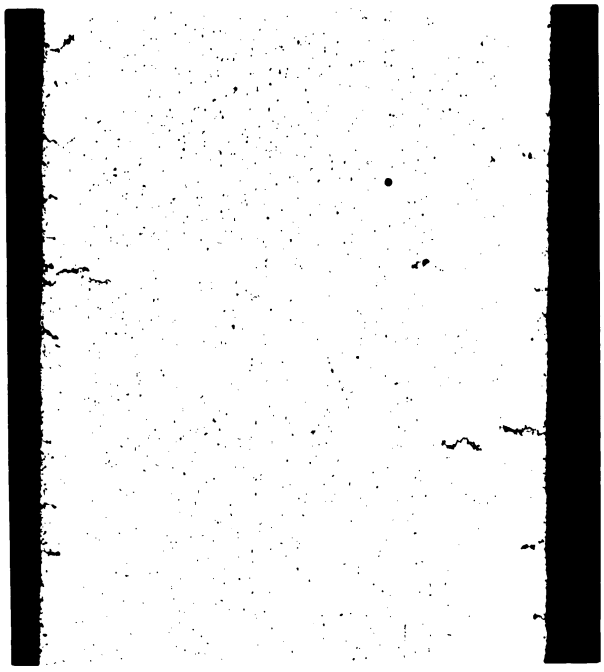

Fig. 3. Slight fissuring in matrix, Chromel ASM alloy, 1900°F, 100 hr, stress 1080 psi, 50x, cross section, unetched.

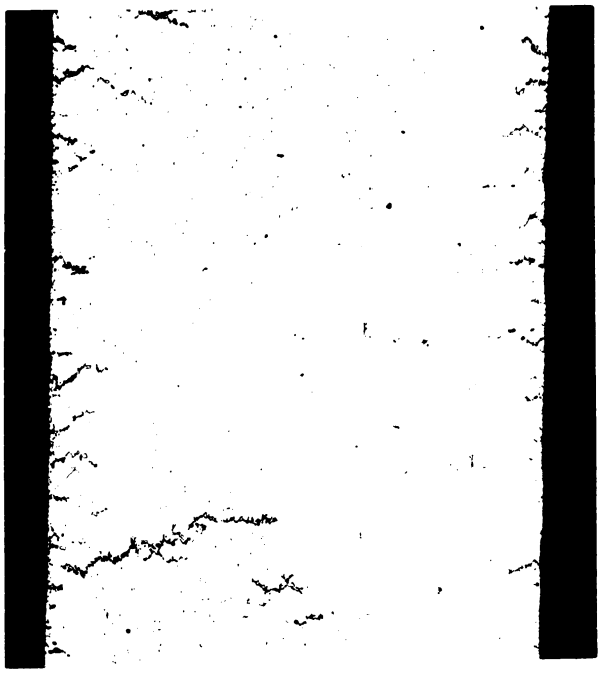

Fig. 4. Fissuring in matrix, Chromel ASM alloy, 1900°F, 100 hr, stress 1125 psi, 50x, cross section, unetched.

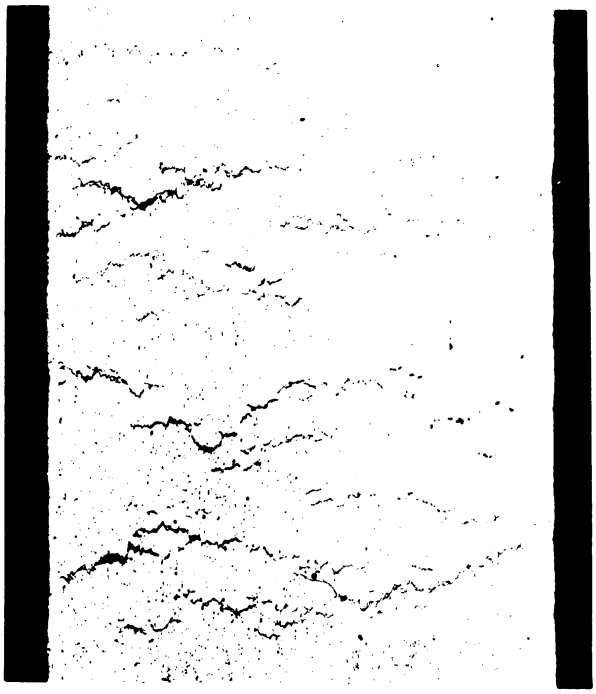

Fig. 5. Fissuring throughout matrix, Chromel ASM alloy, 1700°F, 100 hr, stress 2240 psi, 50x, cross section, unetched.

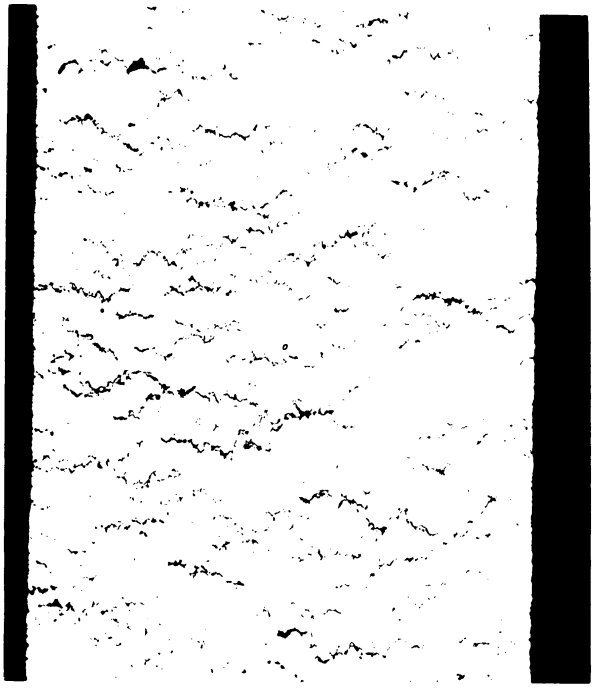

Fig. 6. Fissuring throughout matrix, Chromel ASM alloy, 1800°F, 100 hr, stress 1600 psi, 50x, cross section, unetched.

Fig. 7. Fissuring throughout matrix, Chromel ARM alloy, heat A, 1800°F, 100 hr, stress 2000 psi, 50x, cross section, unetched.

Fig. 8. Fissuring throughout matrix, Chromel ARM alloy, heat A, 2000°F, 100 hr, stress 1000 psi, 50x, cross section, unetched.

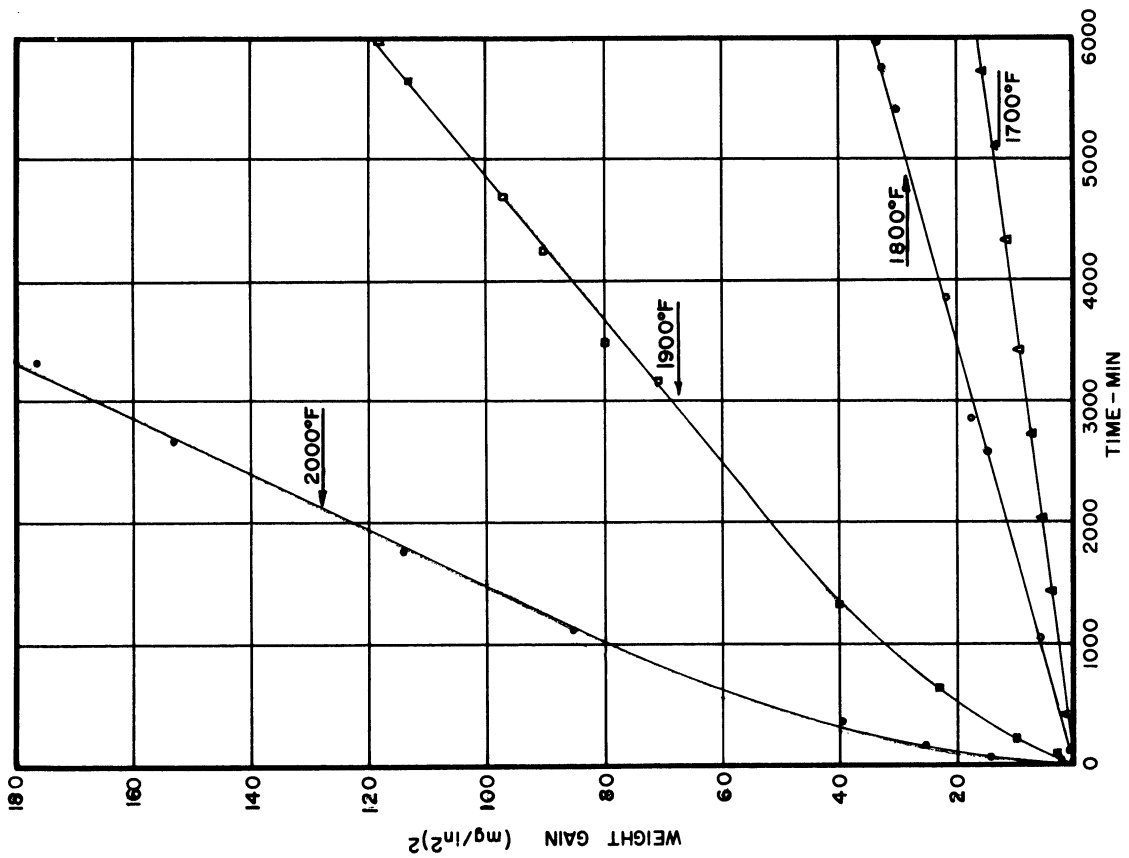

Fig. 10. Application of parabolic relationship to weight-gain data; type 310 alloy, heat 25139.

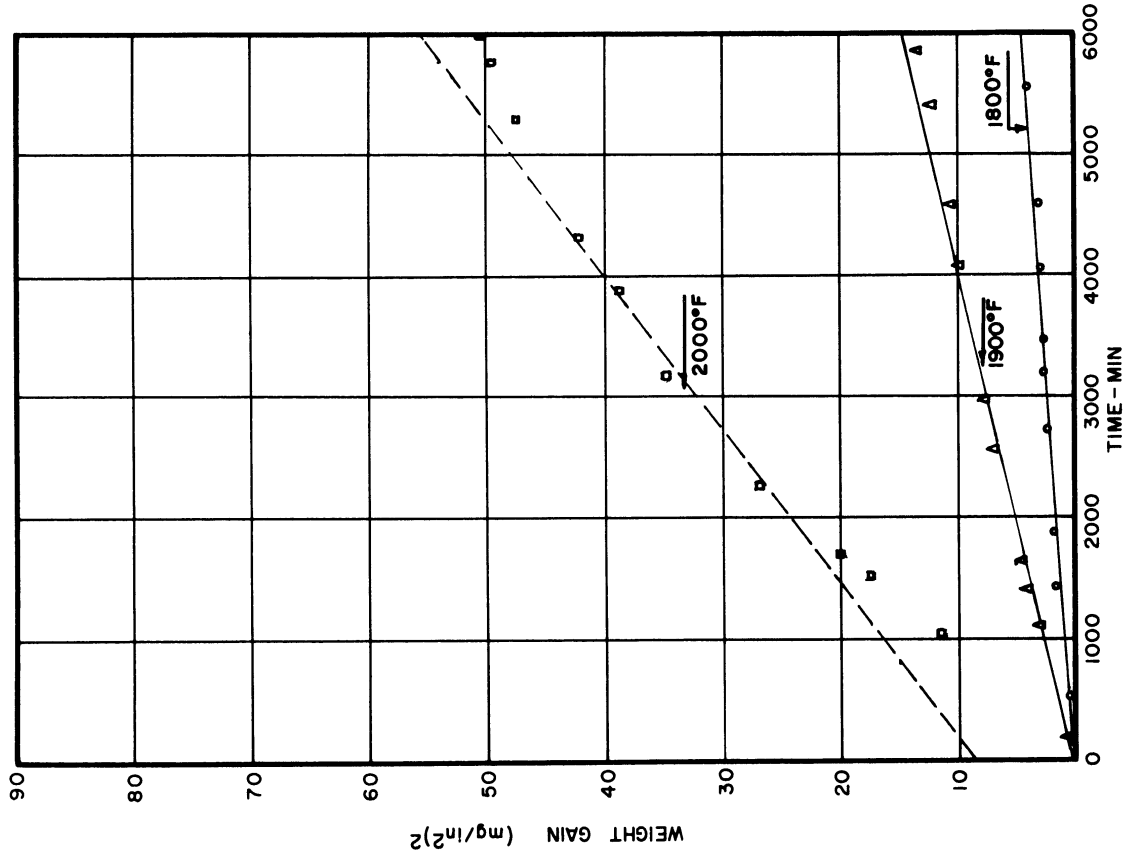

Fig. 9. Application of parabolic relationship to weight-gain data; Chromel ASM alloy.

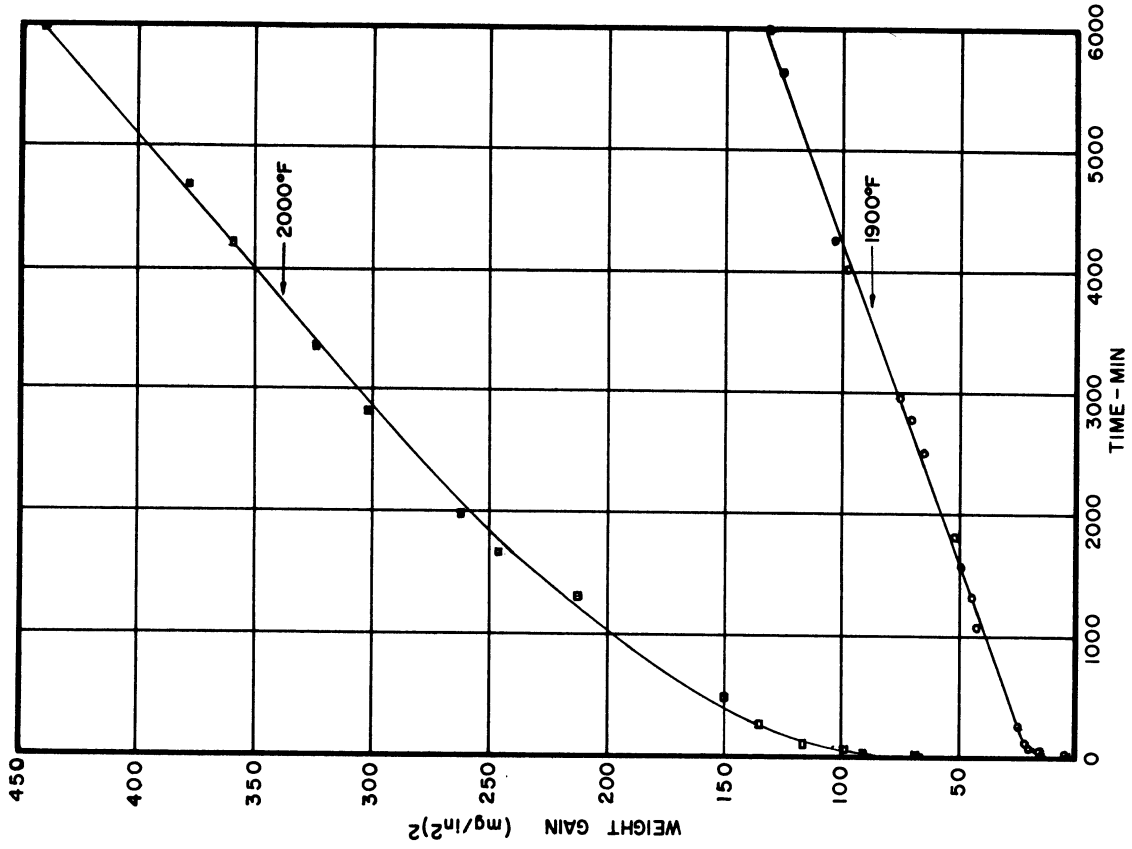

Fig. 12. Application of parabolic relationship to weight-gain data; type 310 alloy, heat 4X-343.

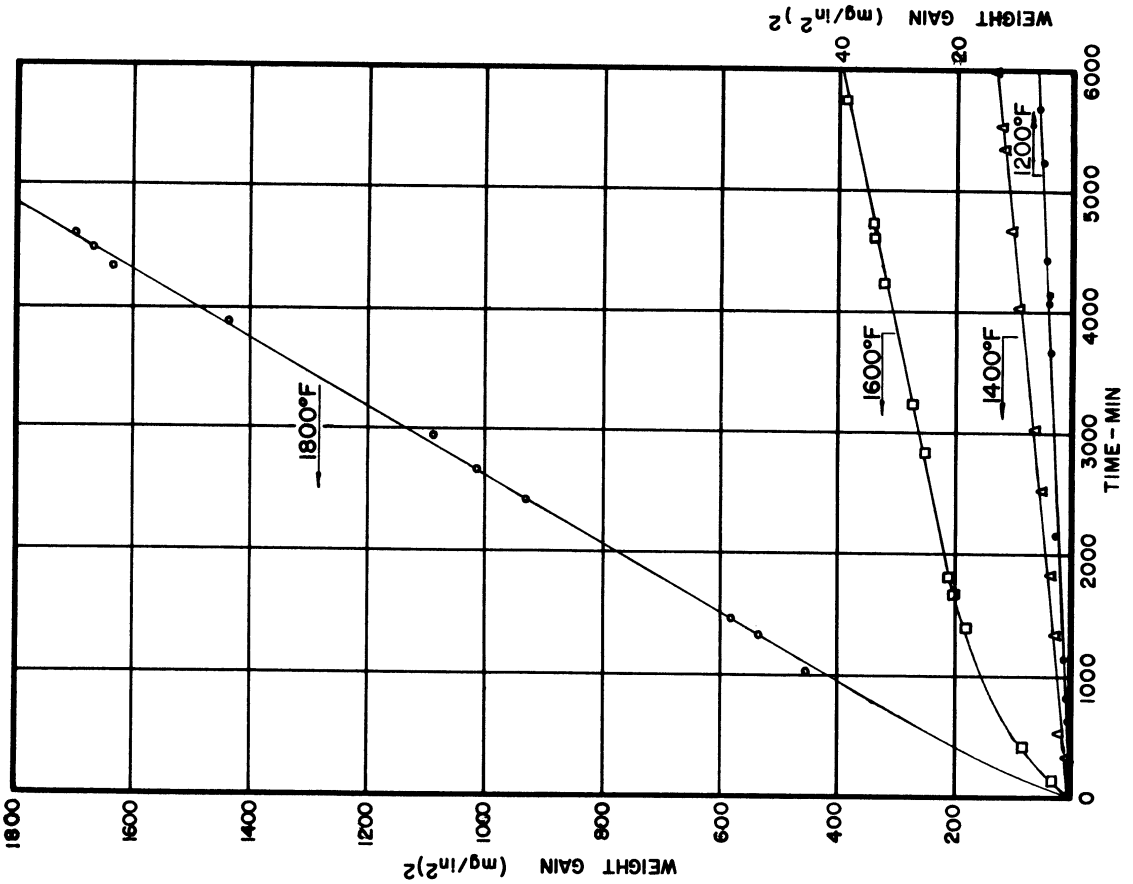

Fig. 11. Application of parabolic relationship to weight-gain data; Hastelloy B, heat B-1400.

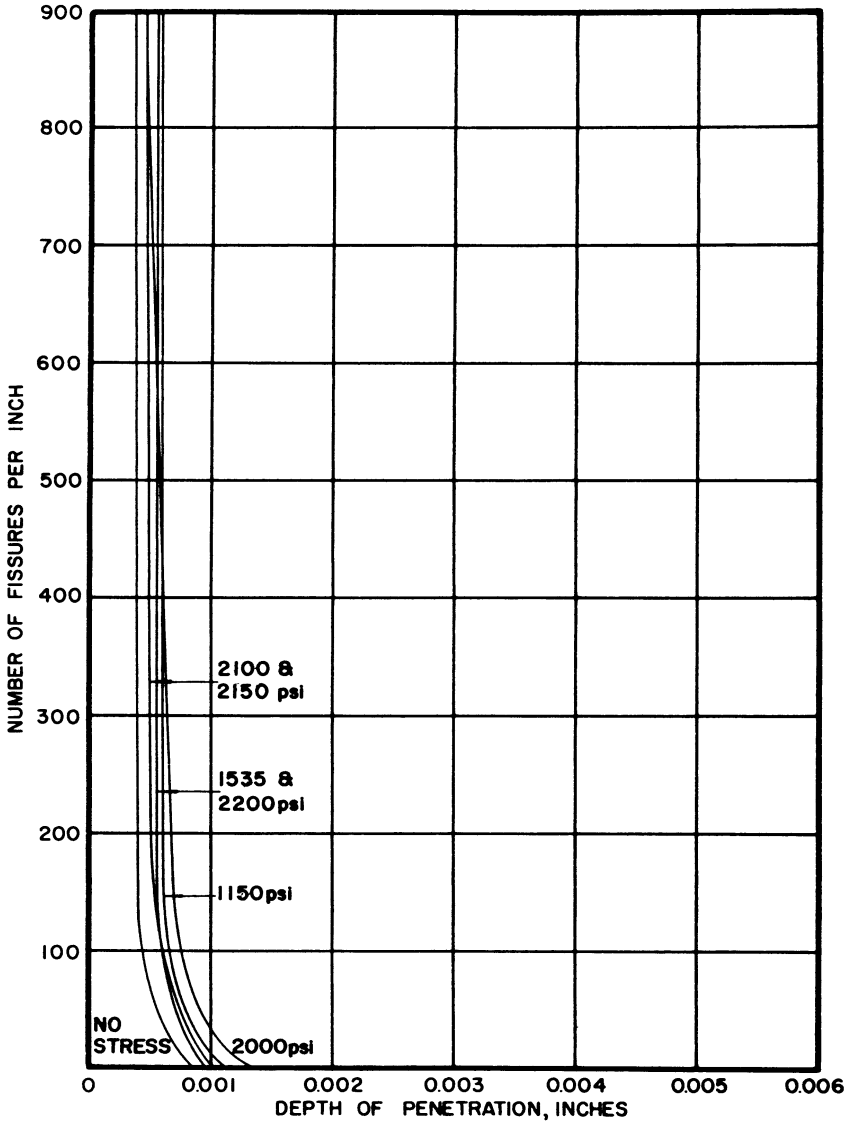

Fig. 13. Penetration vs depth below surface. Chromel ASM alloy. 1700°F, 100 hours.

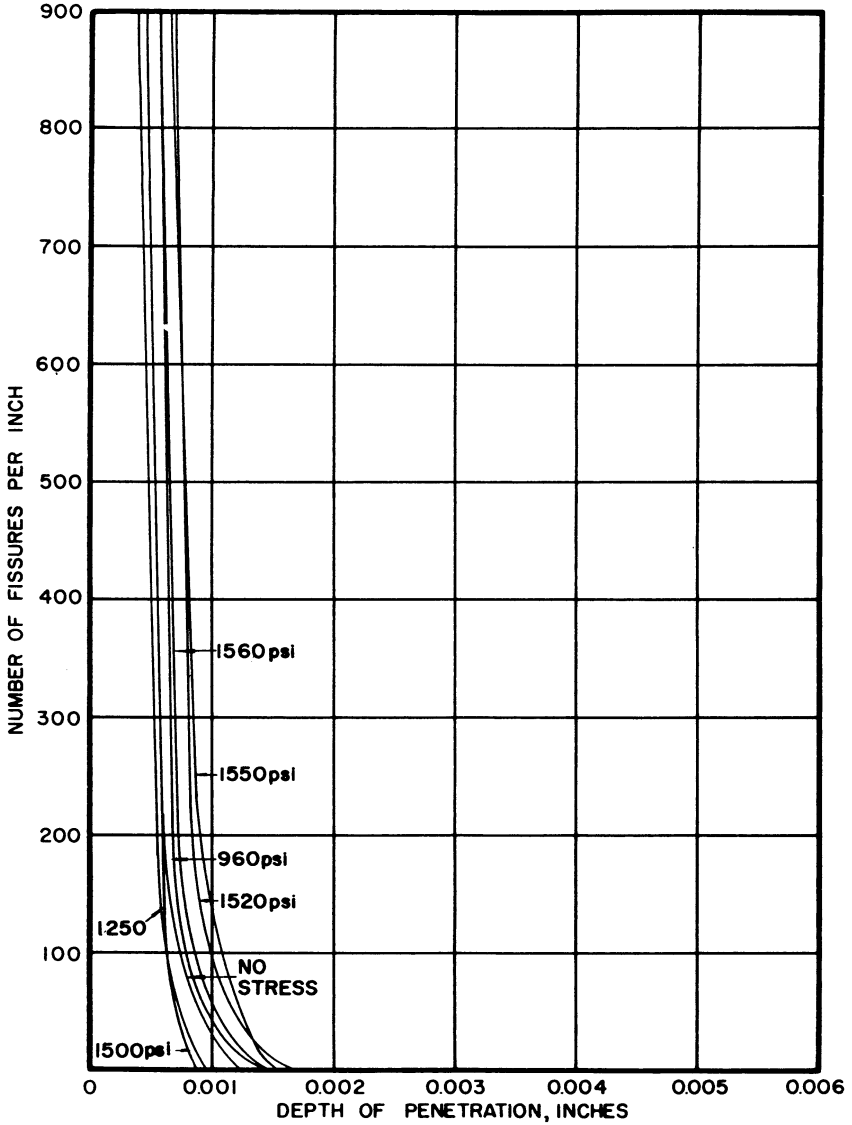

Fig. 14. Penetration vs depth below surface. Chromel ASM alloy. 1800°F, 100 hours.

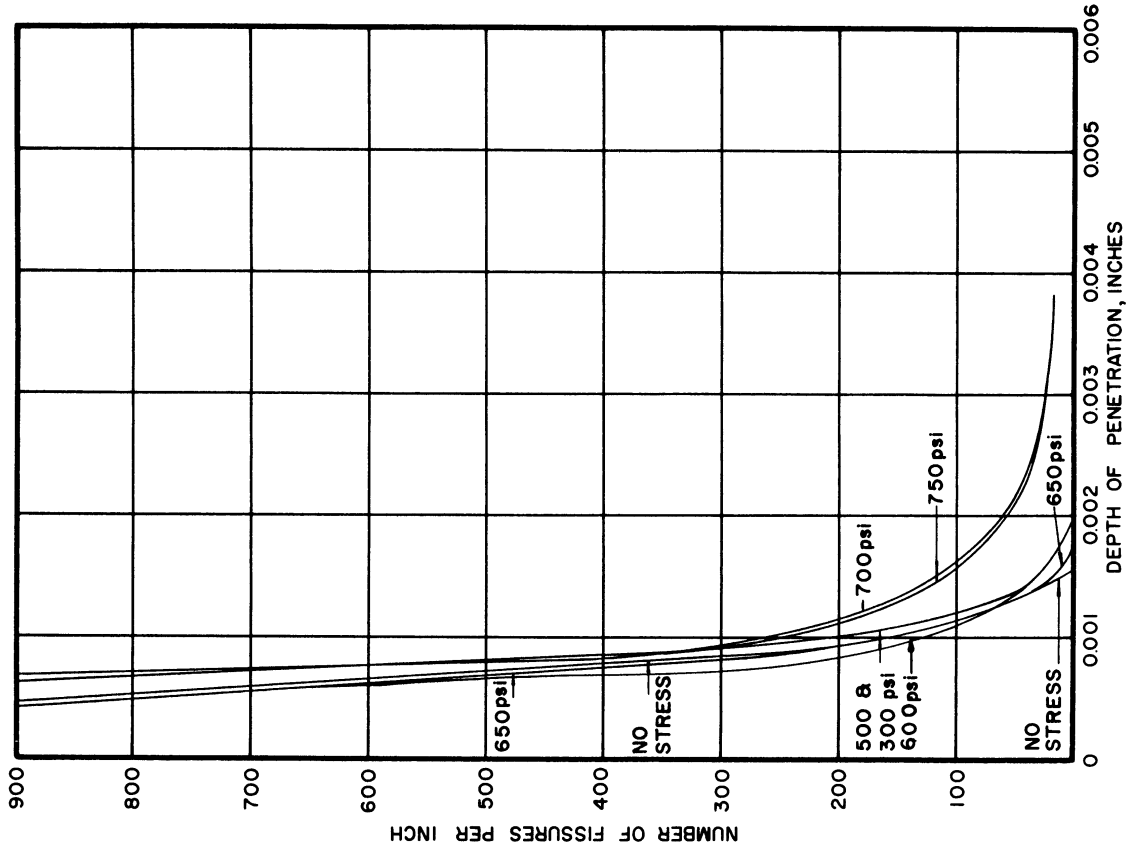

Fig. 16. Penetration vs depth below surface. Chromel ASM alloy. 2000°F, 100 hours.

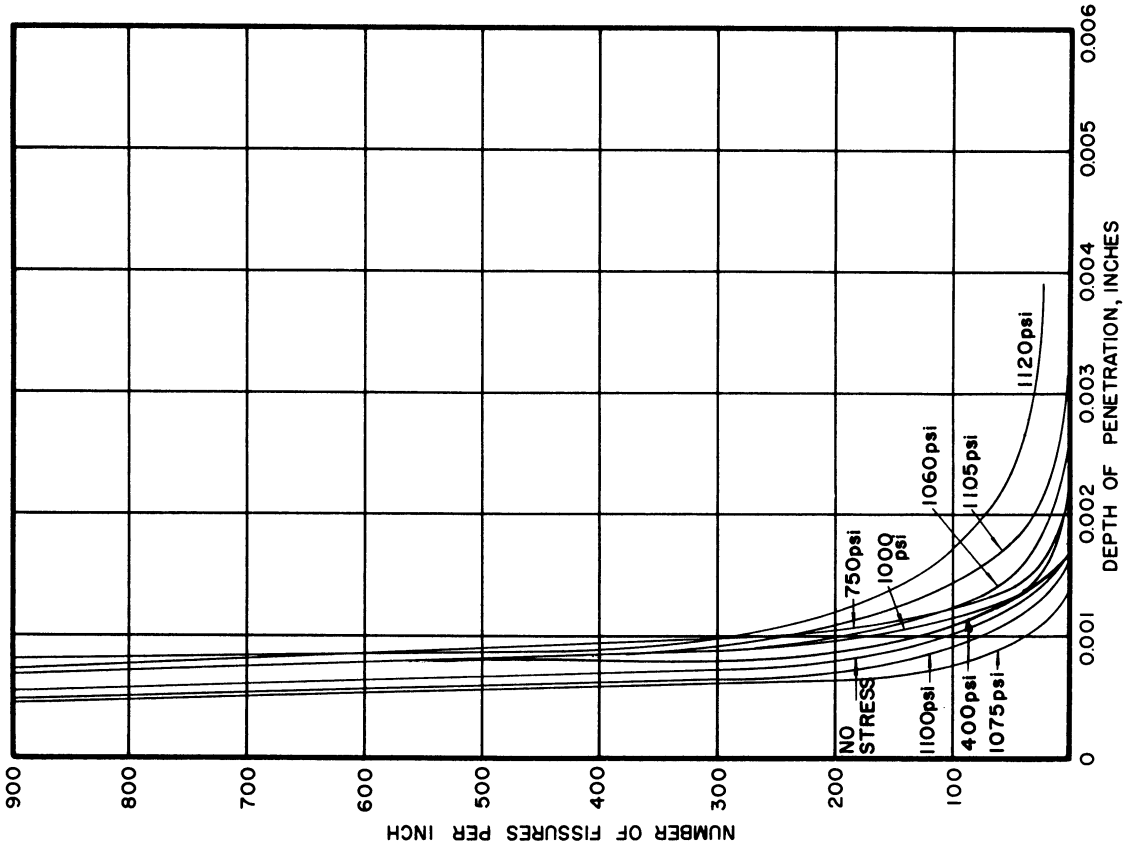

Fig. 15. Penetration vs depth below surface. Chromel ASM alloy. 1900°F, 100 hours.

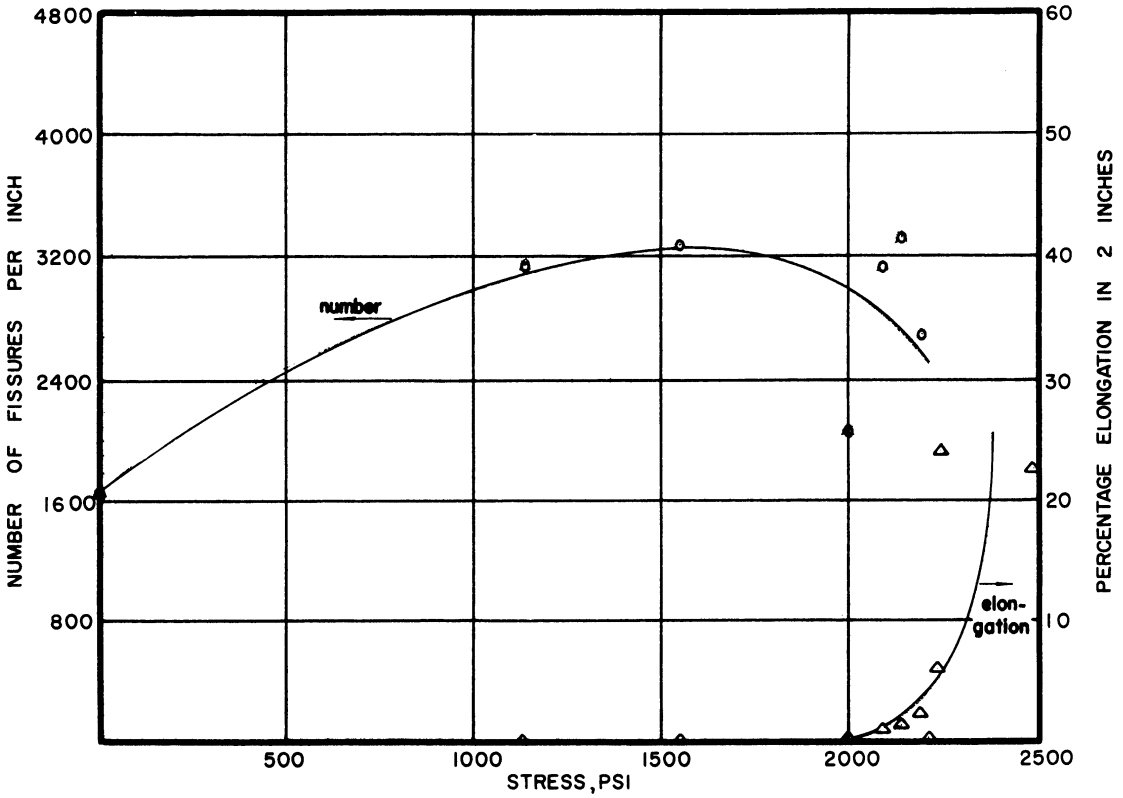

Fig. 17. Summary penetration-frequency curves.
Chromel ASM alloy. 1700°F, 100 hours.

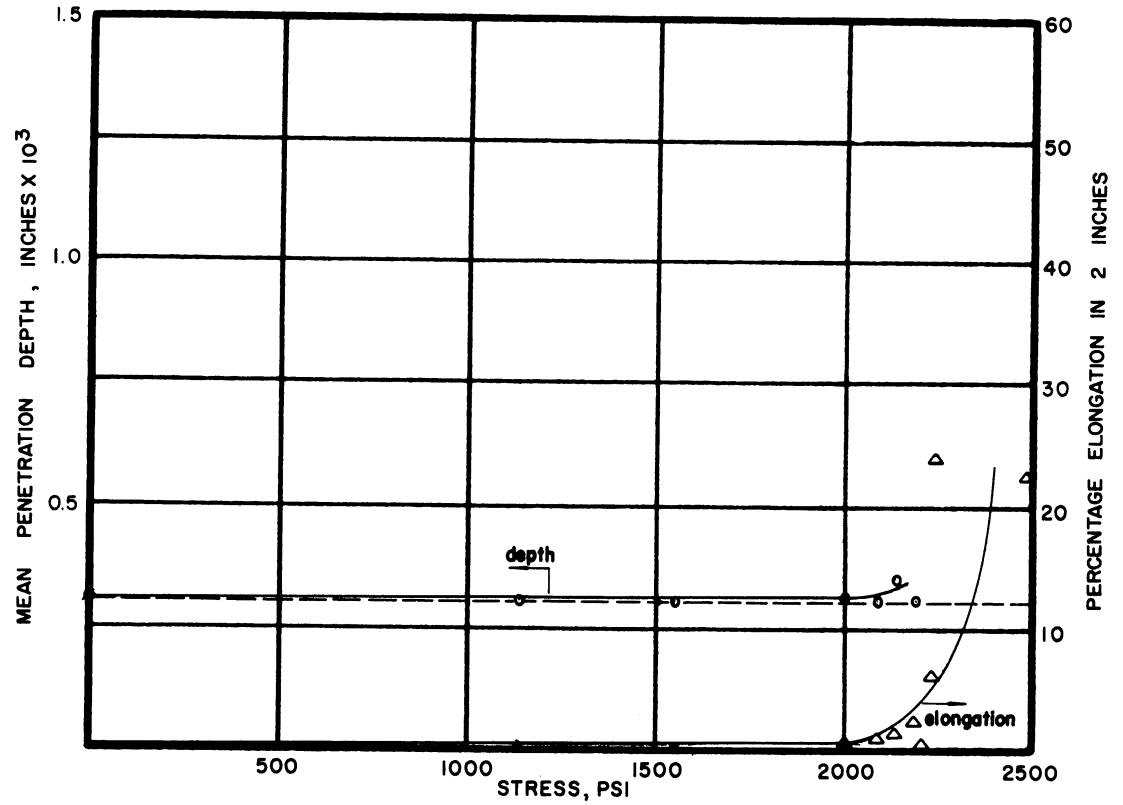

Fig. 18. Summary penetration-depth curves.
Chromel ASM alloy. 1700°F, 100 hours.

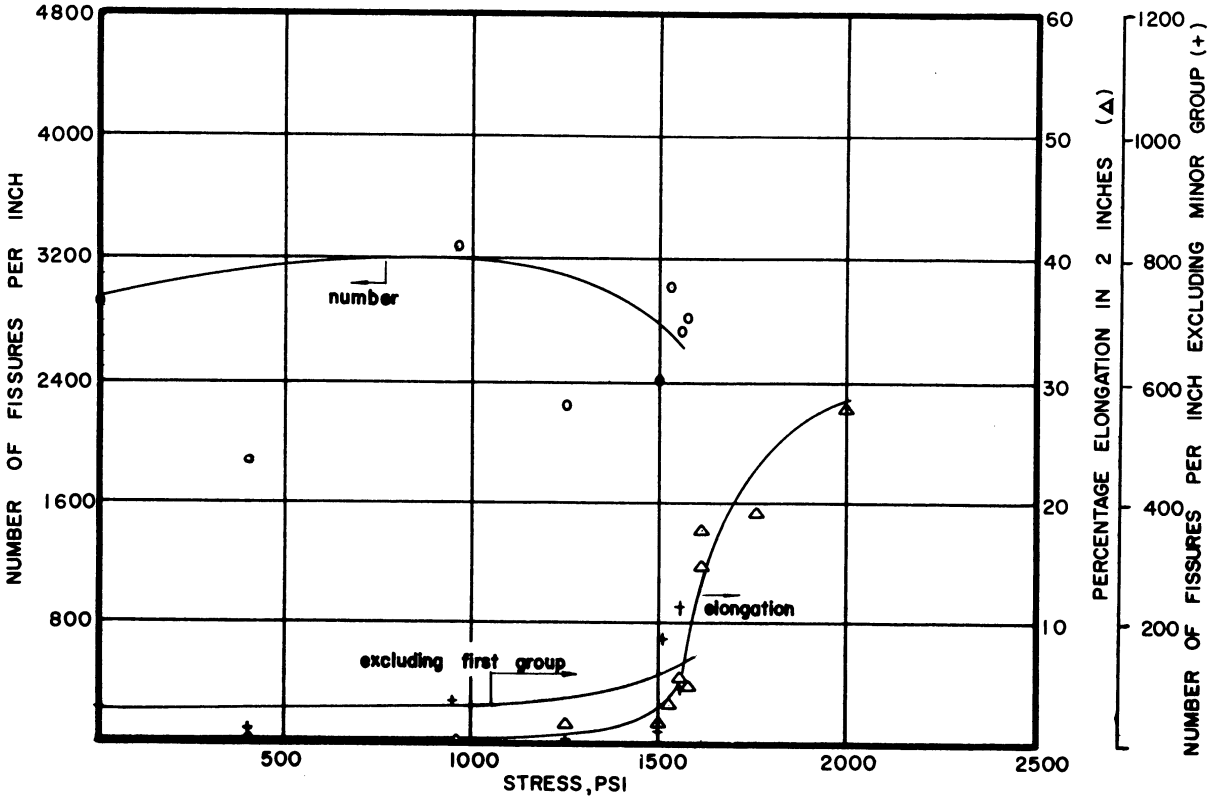

Fig. 19. Summary penetration-frequency curves.
Chromel ASM alloy. 1800°F, 100 hours.

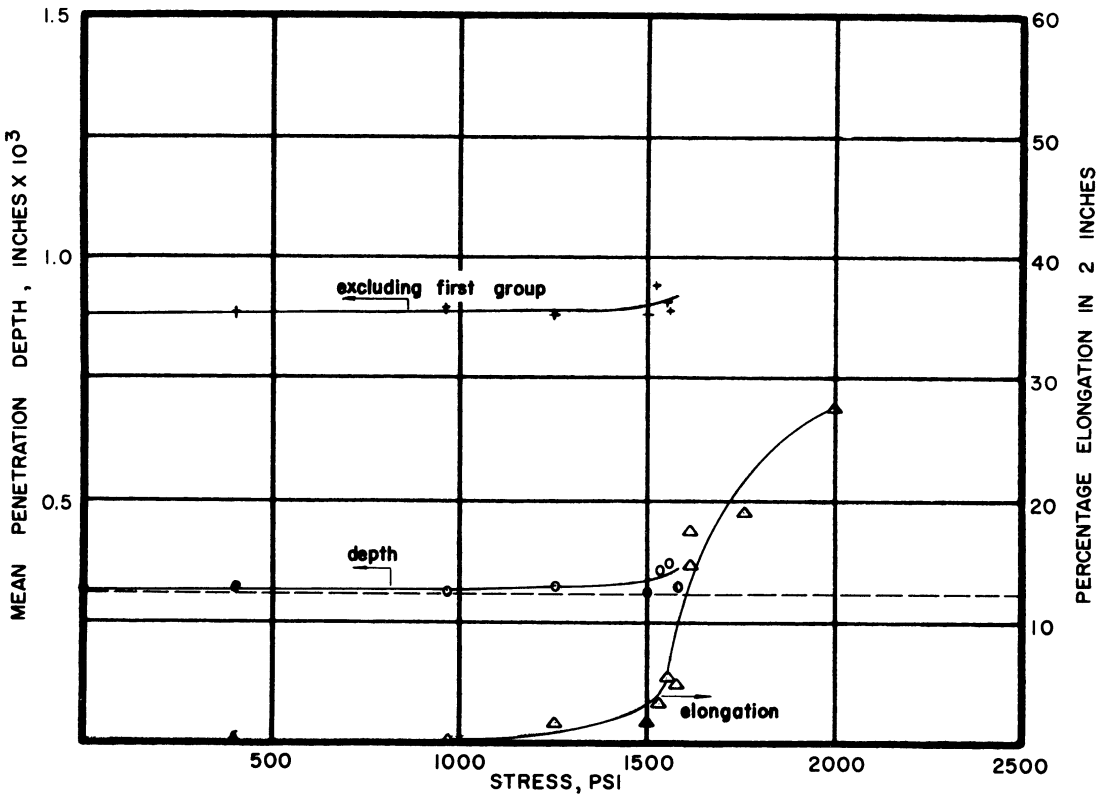

Fig. 20. Summary penetration-depth curves.
Chromel ASM alloy. 1800°F, 100 hours.

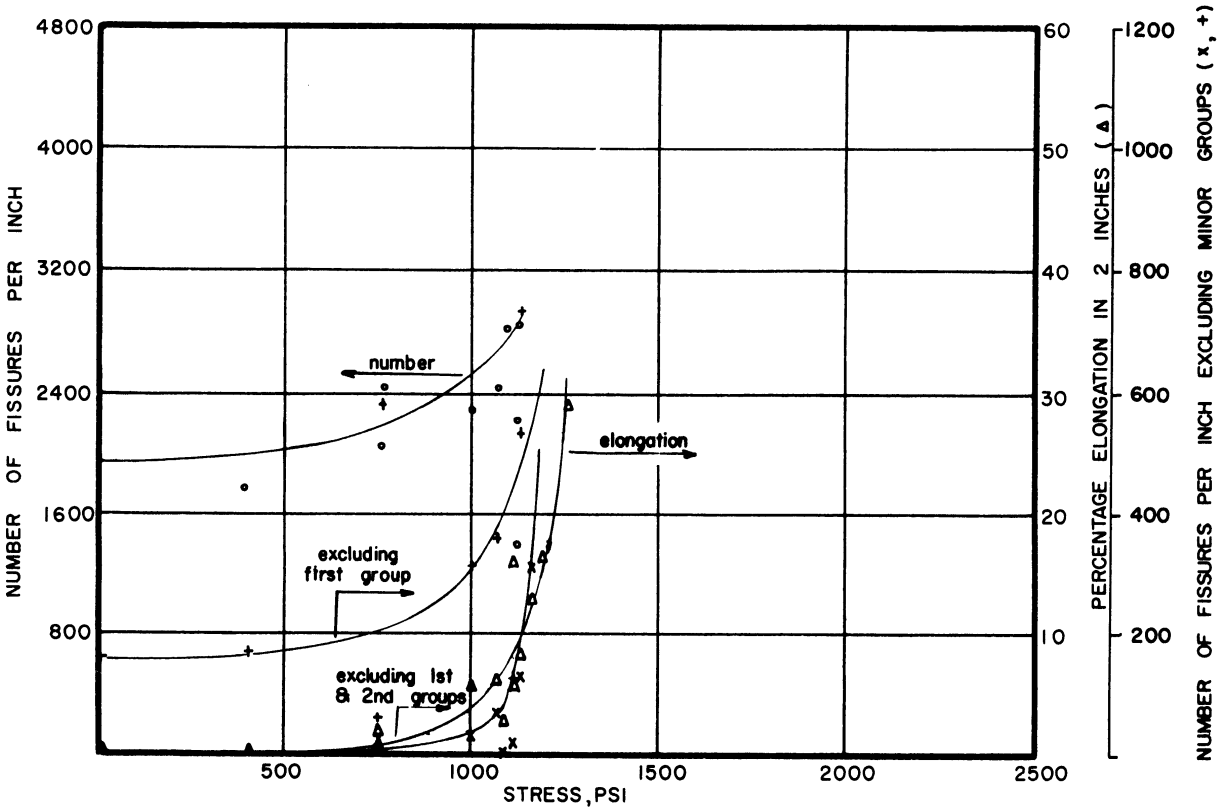

Fig. 21. Summary penetration-frequency curves.
Chromel ASM alloy. 1900°F, 100 hours.

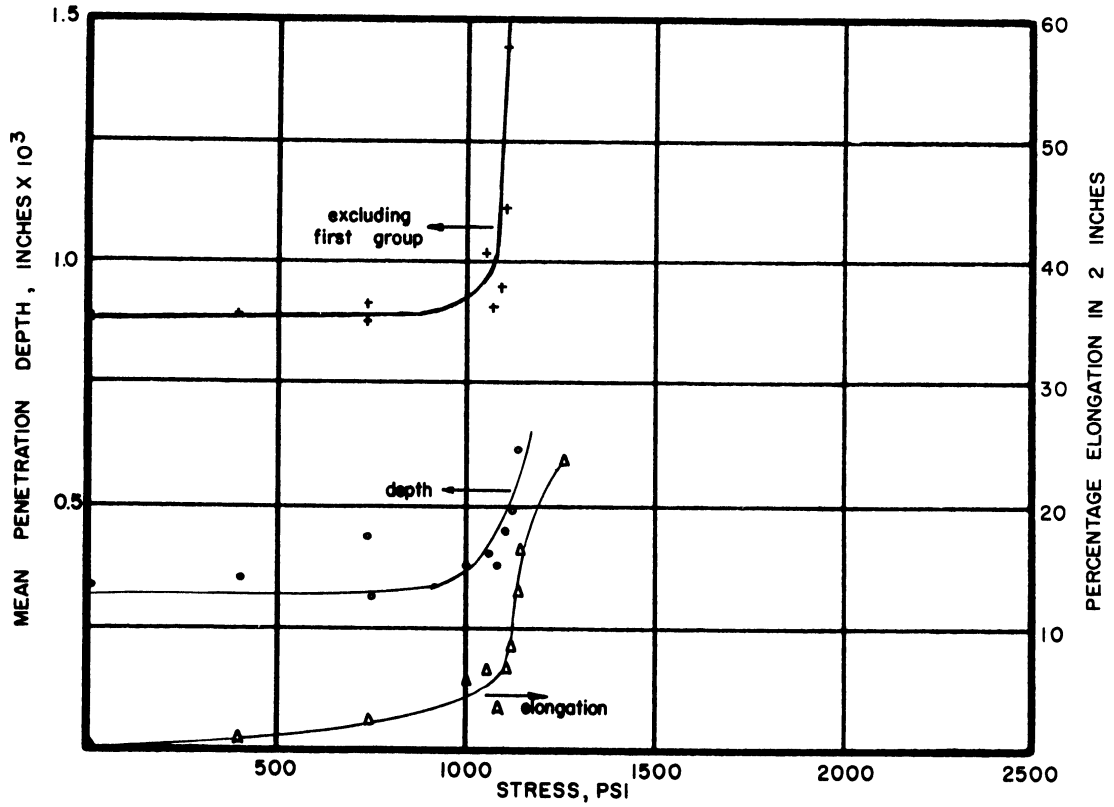

Fig. 22. Summary penetration-depth curves.
Chromel ASM alloy. 1900°F, 100 hours.

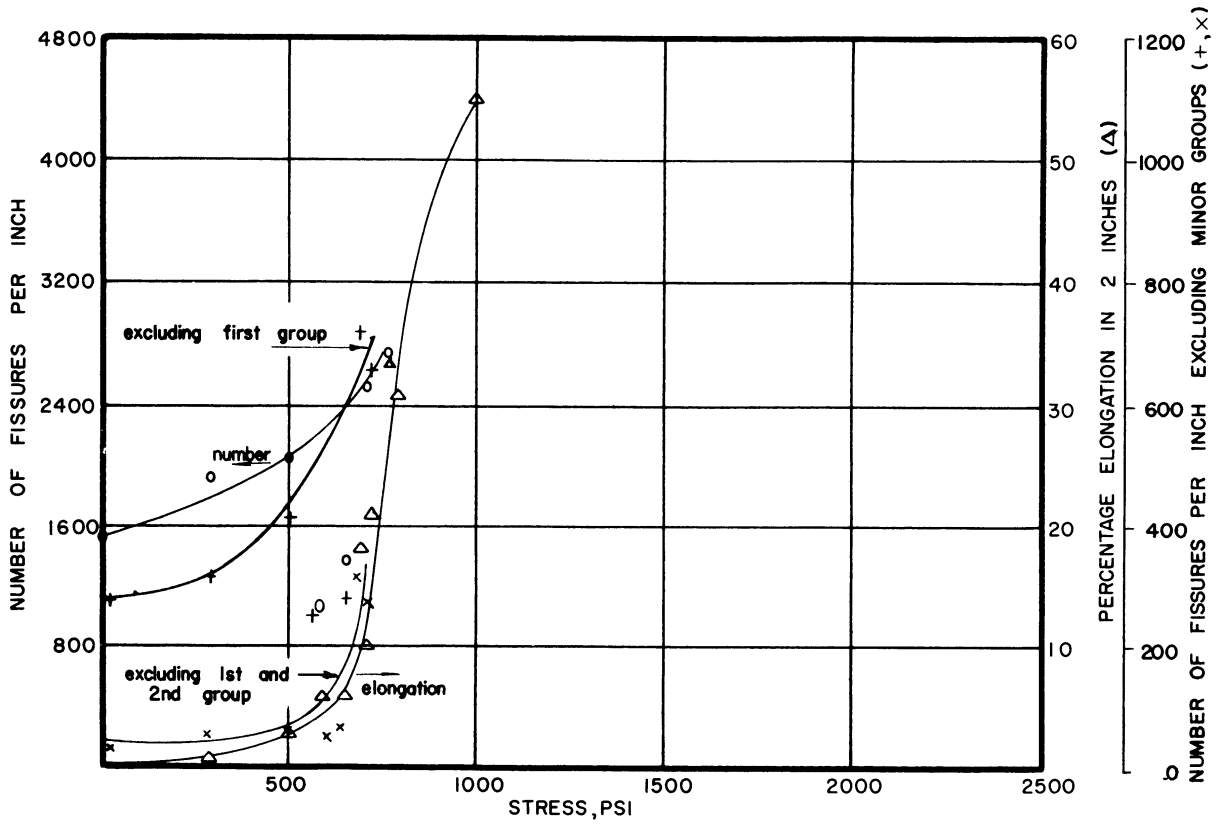

Fig. 23. Summary penetration-frequency curves.
Chromel ASM alloy. 2000°F, 100 hours.

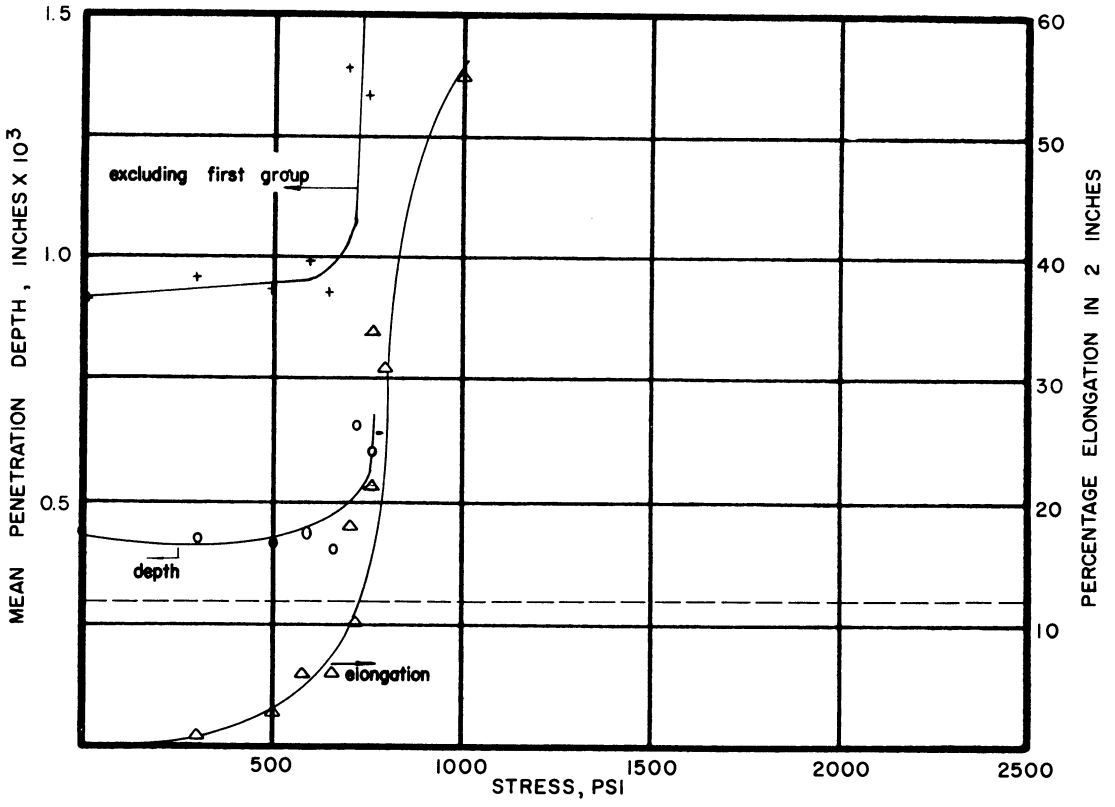

Fig. 24. Summary penetration-depth curves.
Chromel ASM alloy. 2000°F, 100 hours.

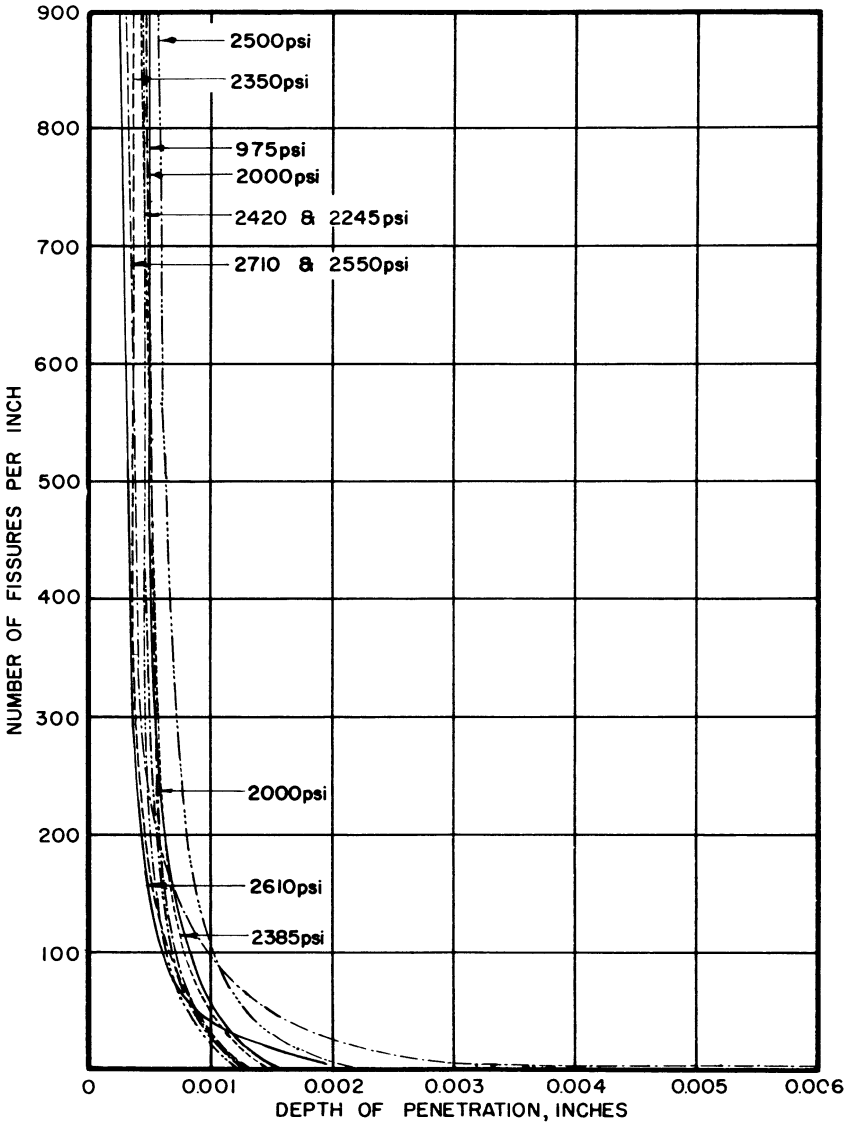

Fig. 25. Penetration vs depth below surface. Type 310 stainless, heat 25139. 1700°F, 100 hours.

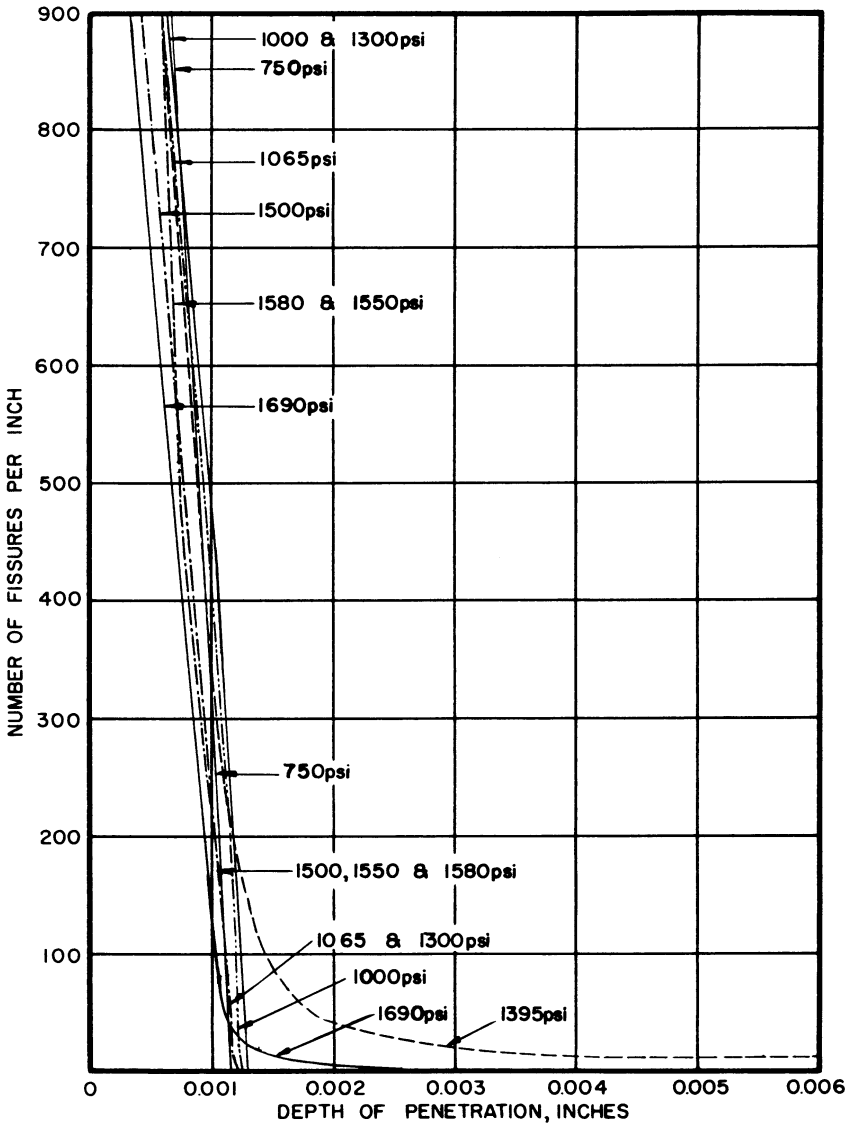

Fig. 26. Penetration vs depth below surface. Type 310 stainless, heat 25139. 1800°F, 100 hours.

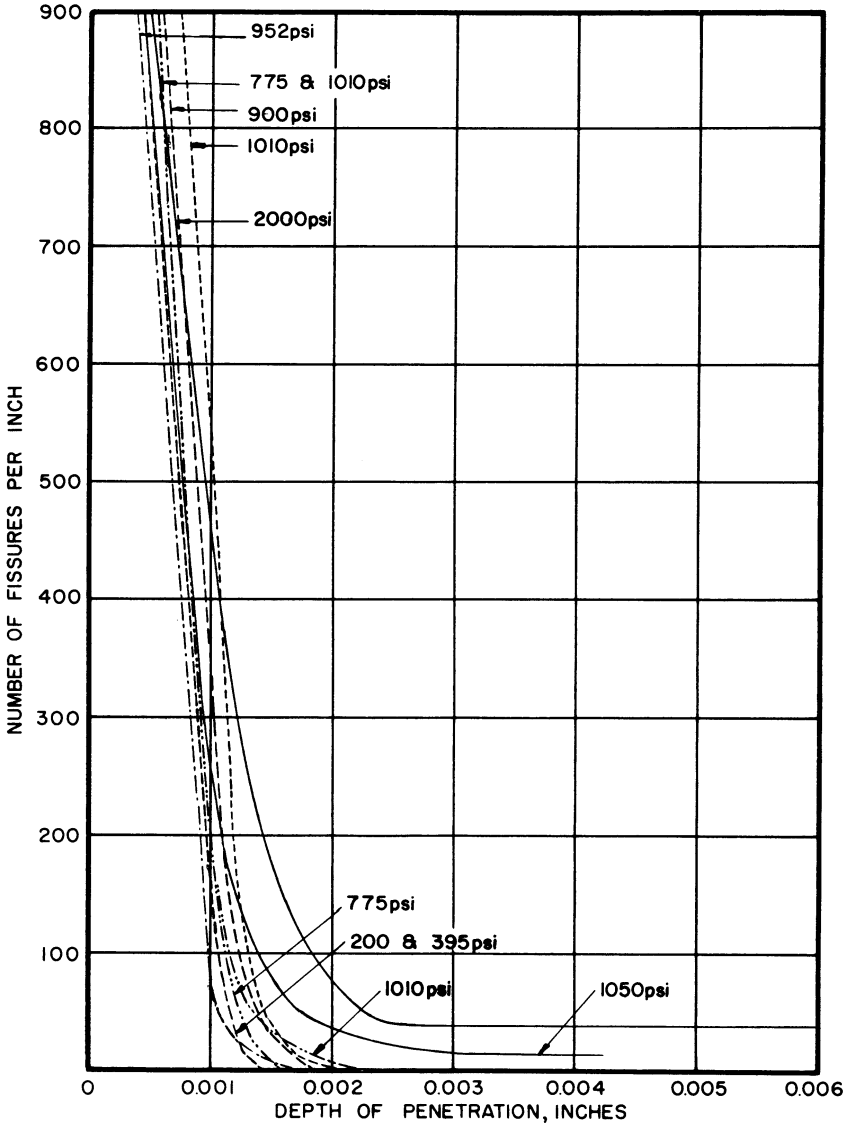

Fig. 27. Penetration vs depth below surface. Type 310 stainless, heat 25139. 1900°F, 100 hours.

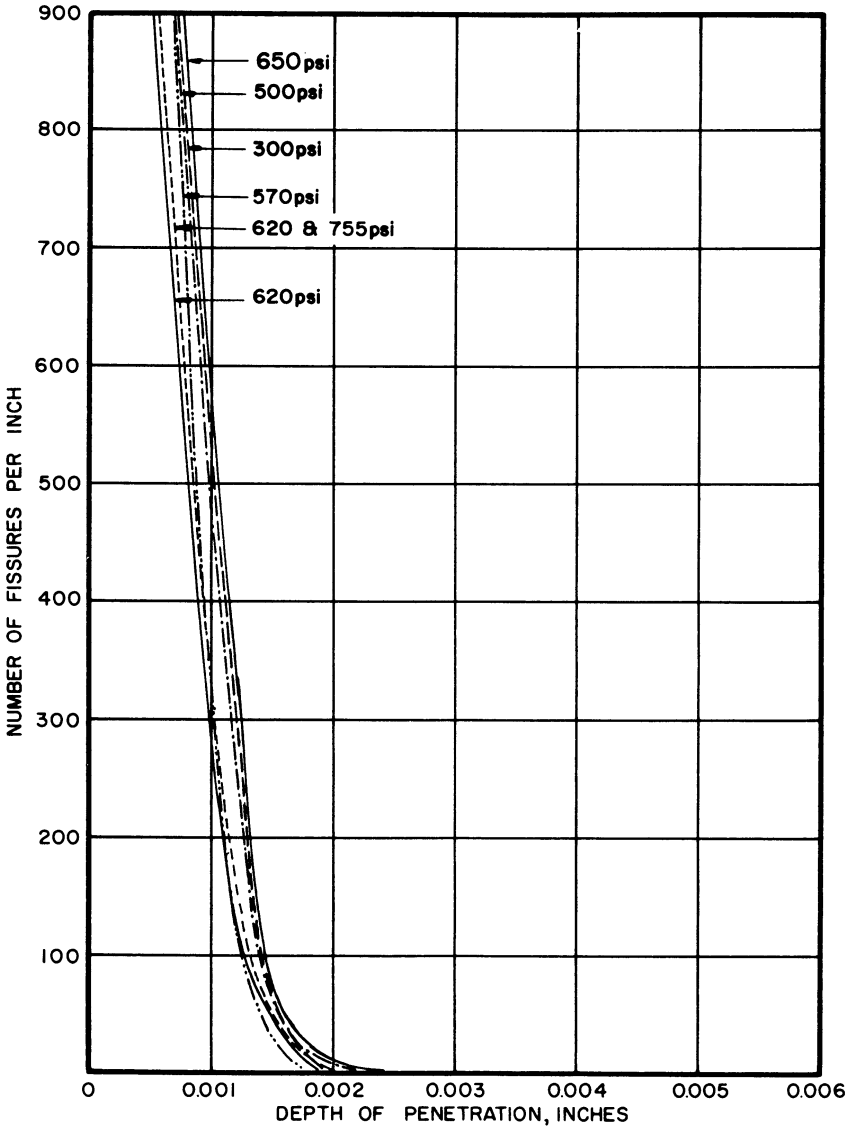

Fig. 28. Penetration vs depth below surface. Type 310 stainless, heat 25139. 2000°F, 100 hours.

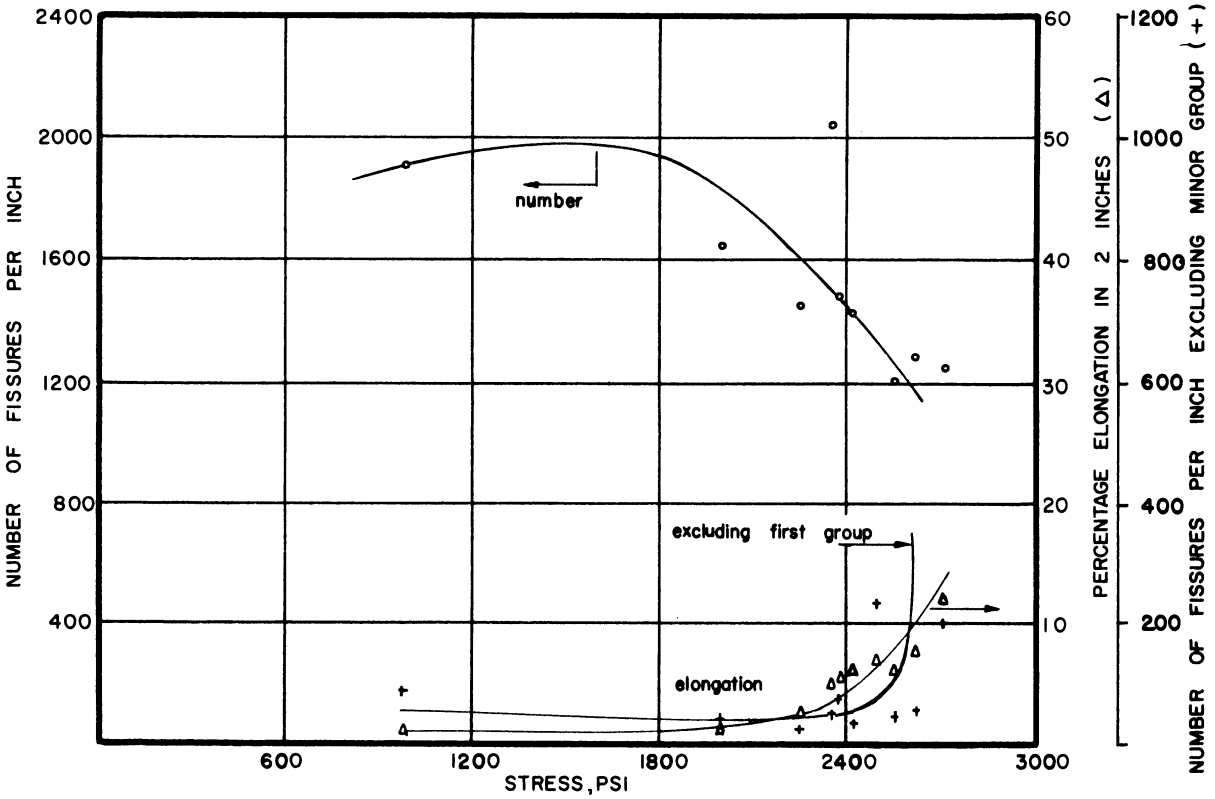

Fig. 29. Summary penetration-frequency curves.
Type 310 alloy, heat 25139. 1700°F, 100 hours.

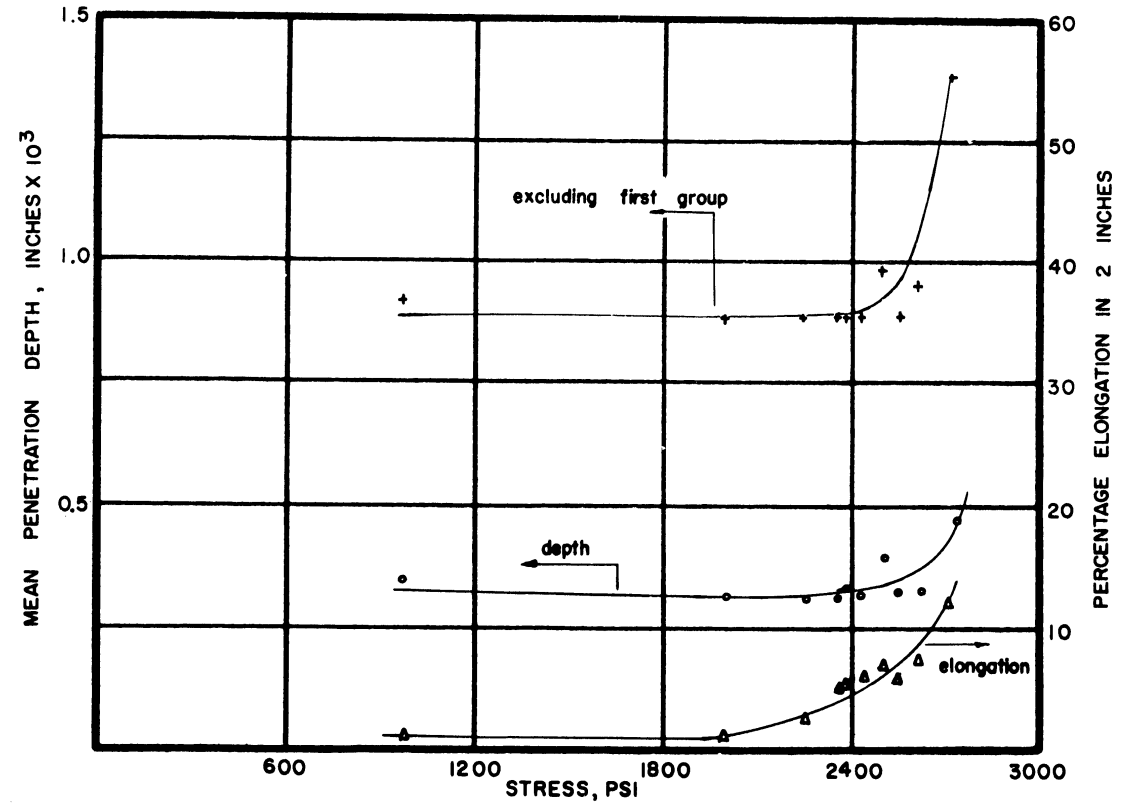

Fig. 30. Summary penetration-depth curves.
Type 310 alloy, heat 25139. 1700°F, 100 hours.

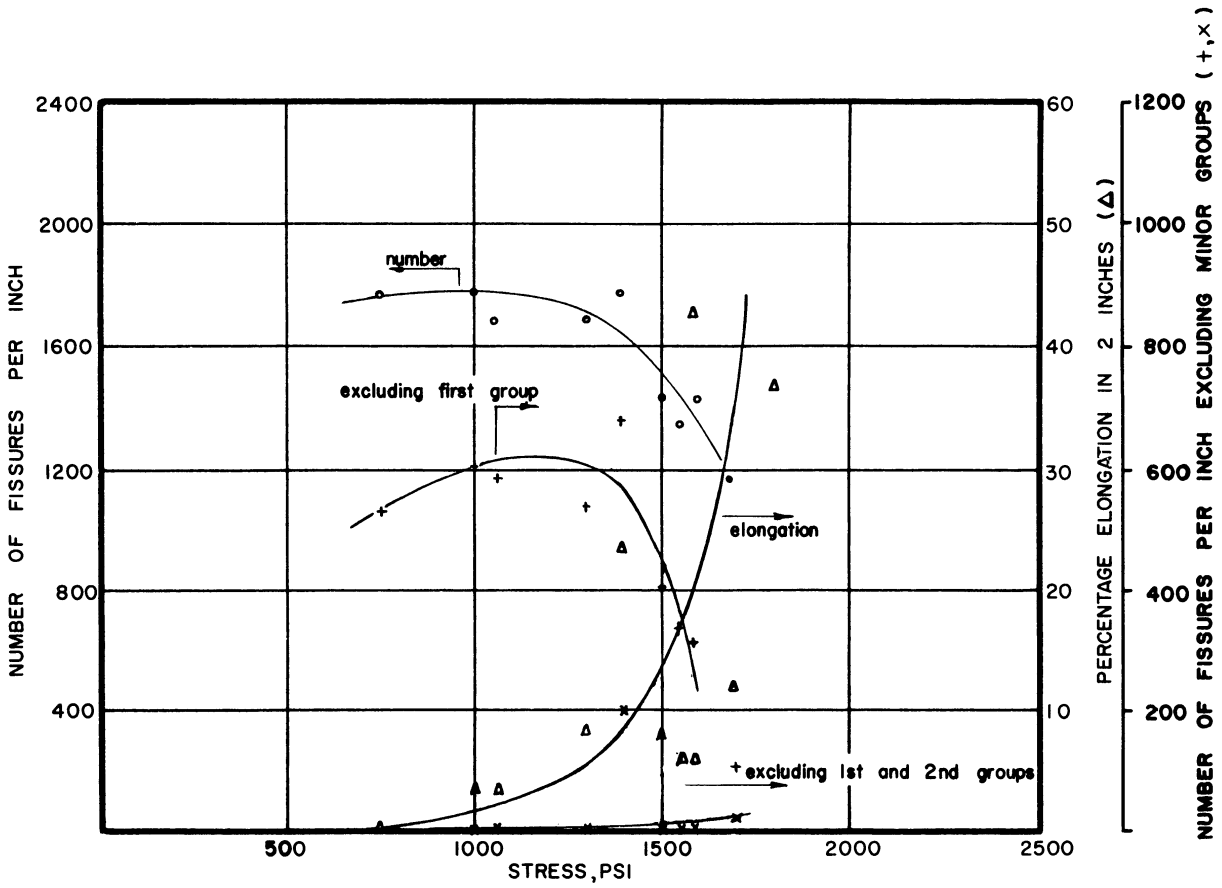

Fig. 31. Summary penetration-frequency curves.
Type 310 alloy, heat 25139. 1800°F, 100 hours.

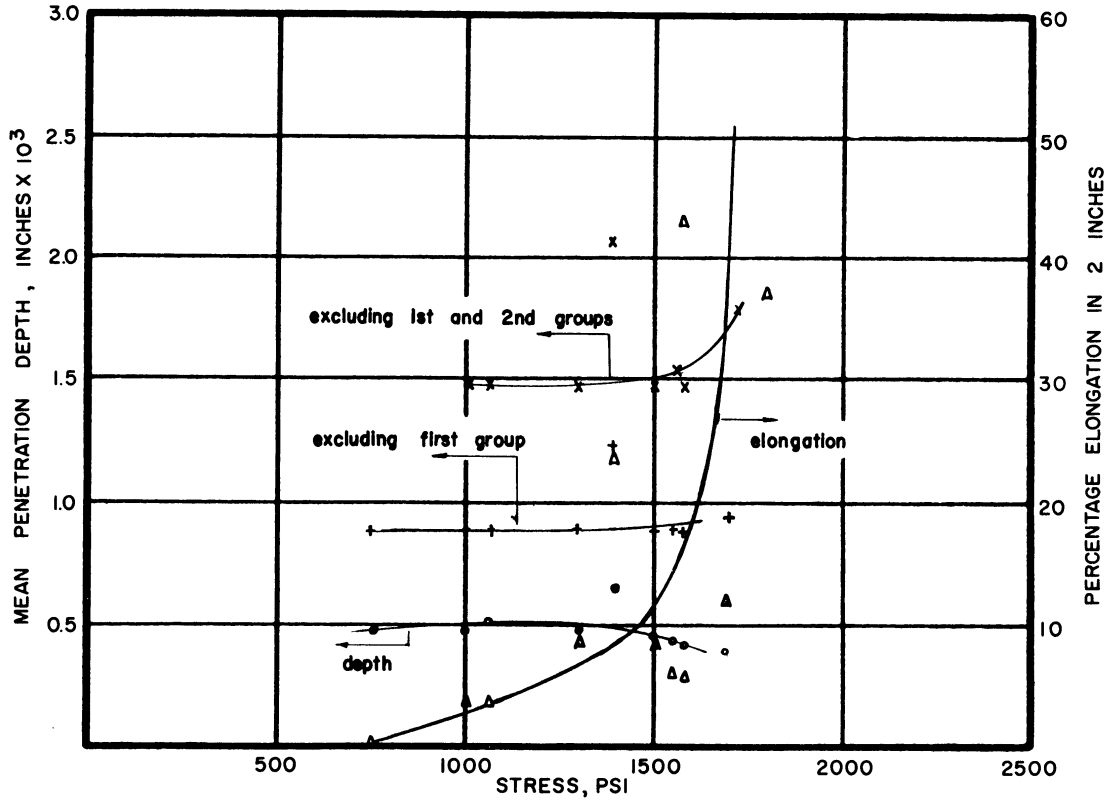

Fig. 32. Summary penetration-depth curves.
Type 310 alloy, heat 25139. 1800°F, 100 hours.

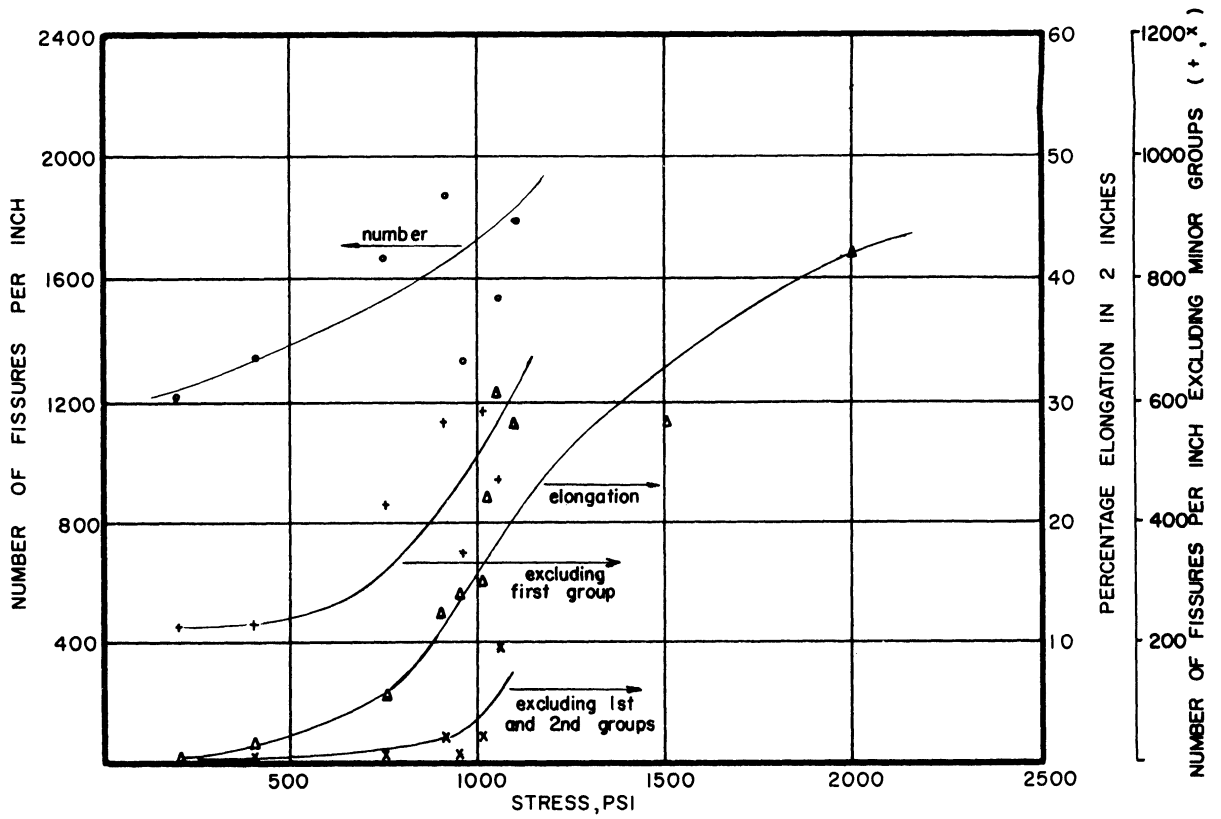

Fig. 33. Summary penetration-frequency curves.
Type 310 alloy, heat 25139. 1900°F, 100 hours.

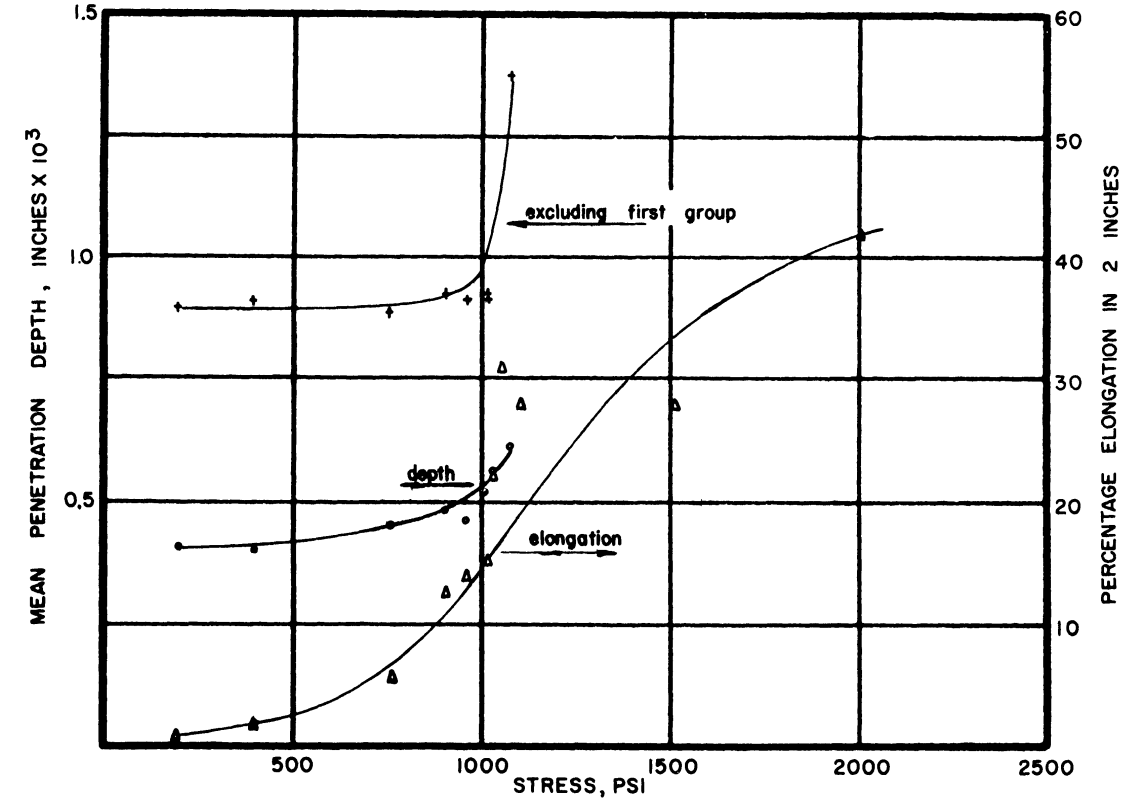

Fig. 34. Summary penetration-depth curves.
Type 310 alloy, heat 25139. 1900°F, 100 hours.

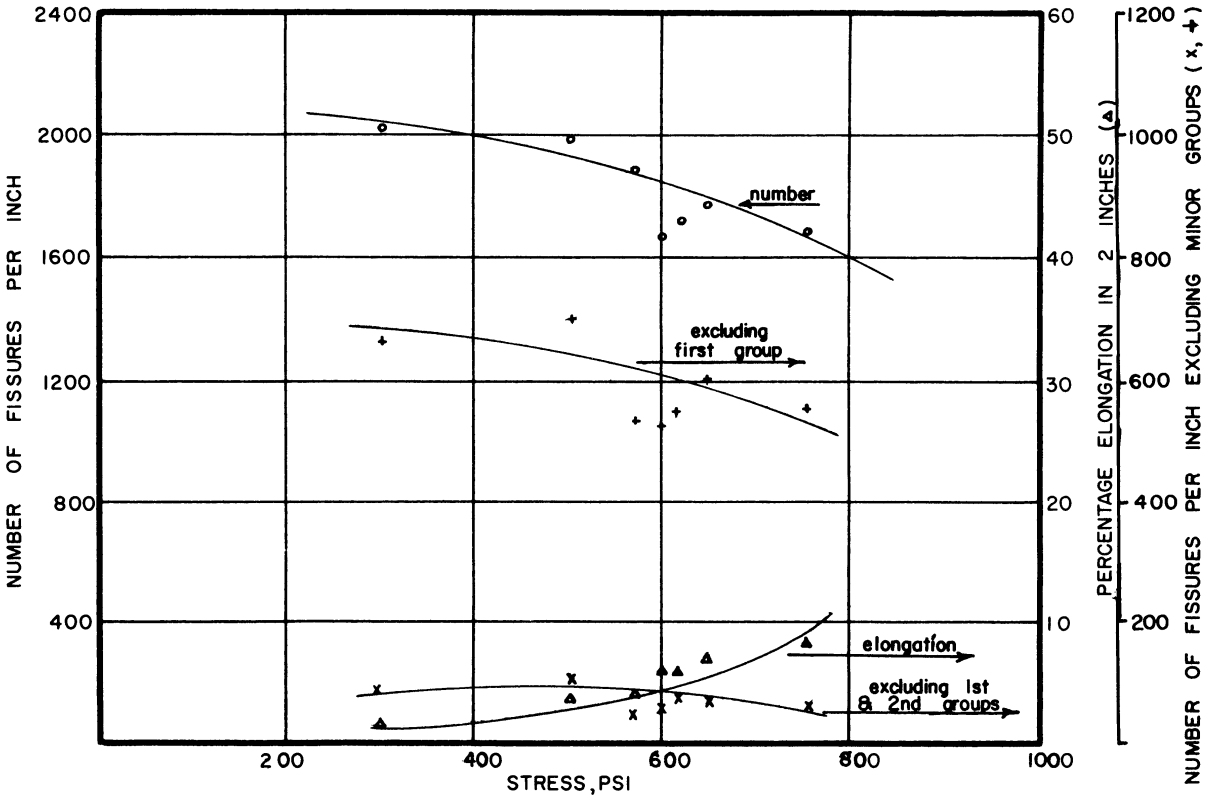

Fig. 35. Summary penetration-frequency curves.
Type 310 alloy, heat 25139. 2000°F, 100 hours.

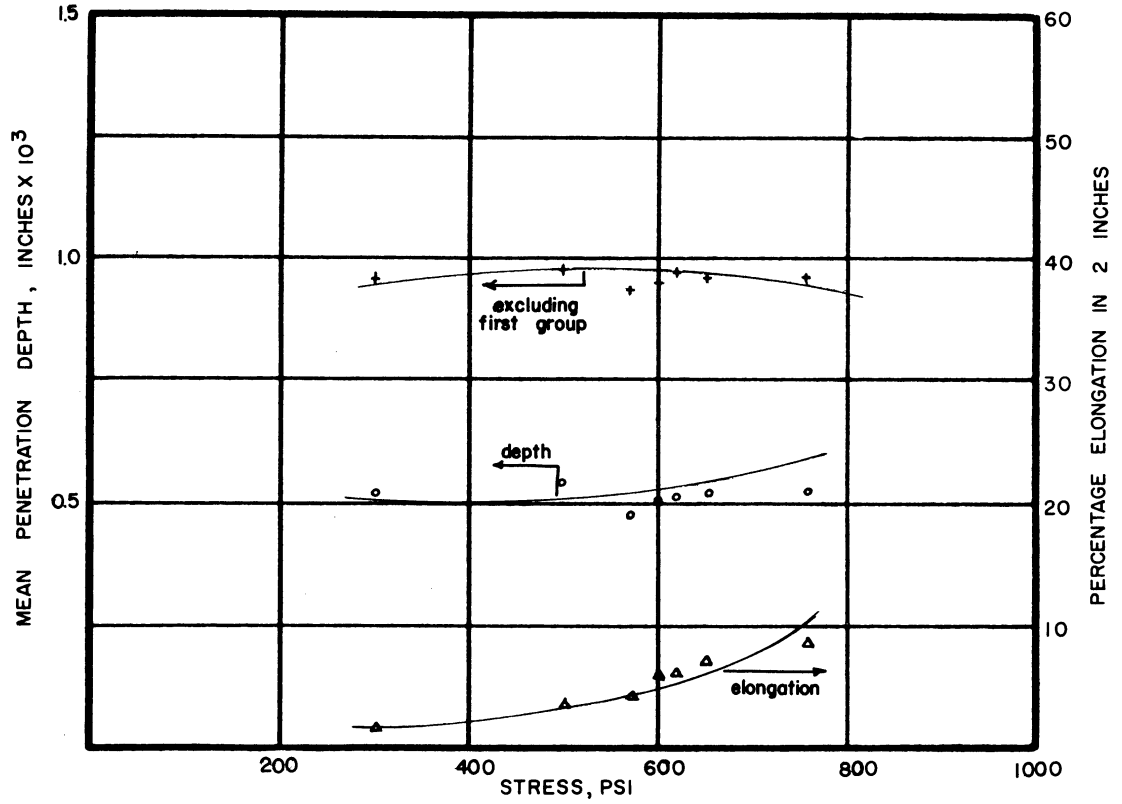

Fig. 36. Summary penetration-depth curves.
Type 310 alloy, heat 25139. 2000°F, 100 hours.

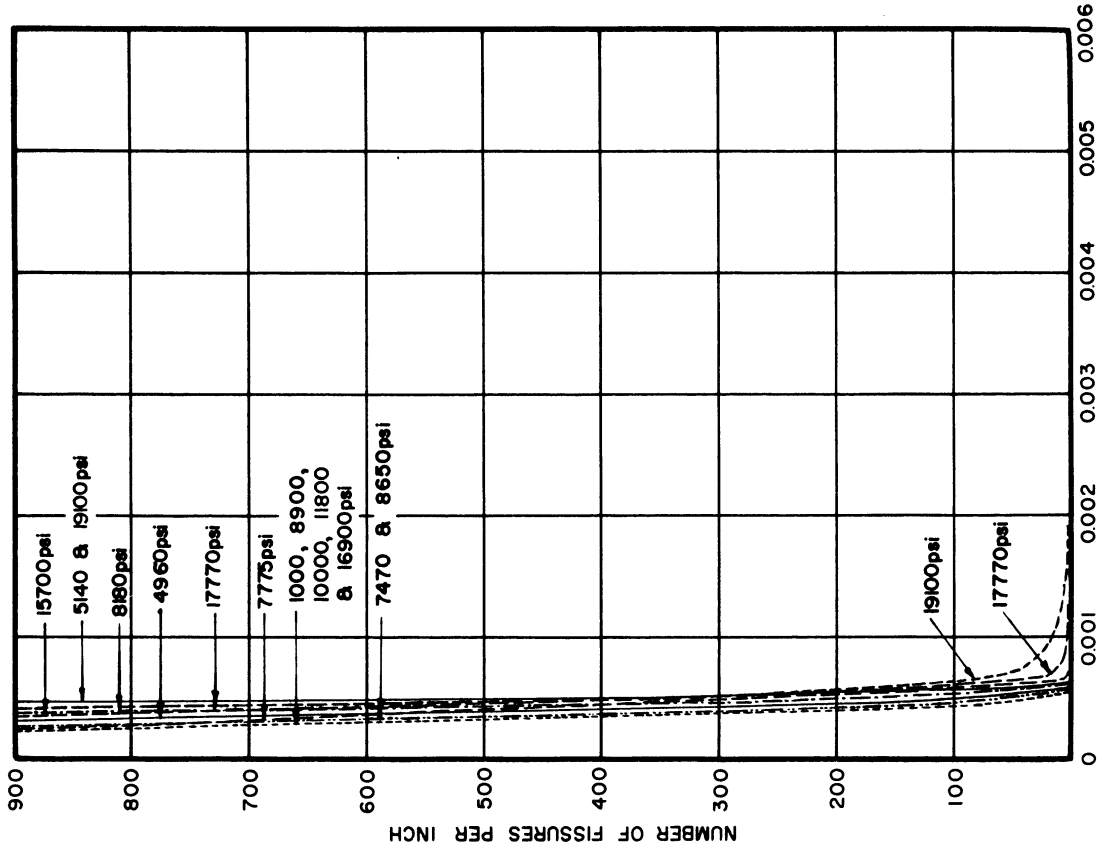

Fig. 38. Penetration vs depth below surface. Hastelloy B, heat B-1400. 1400°F, 100 hours.

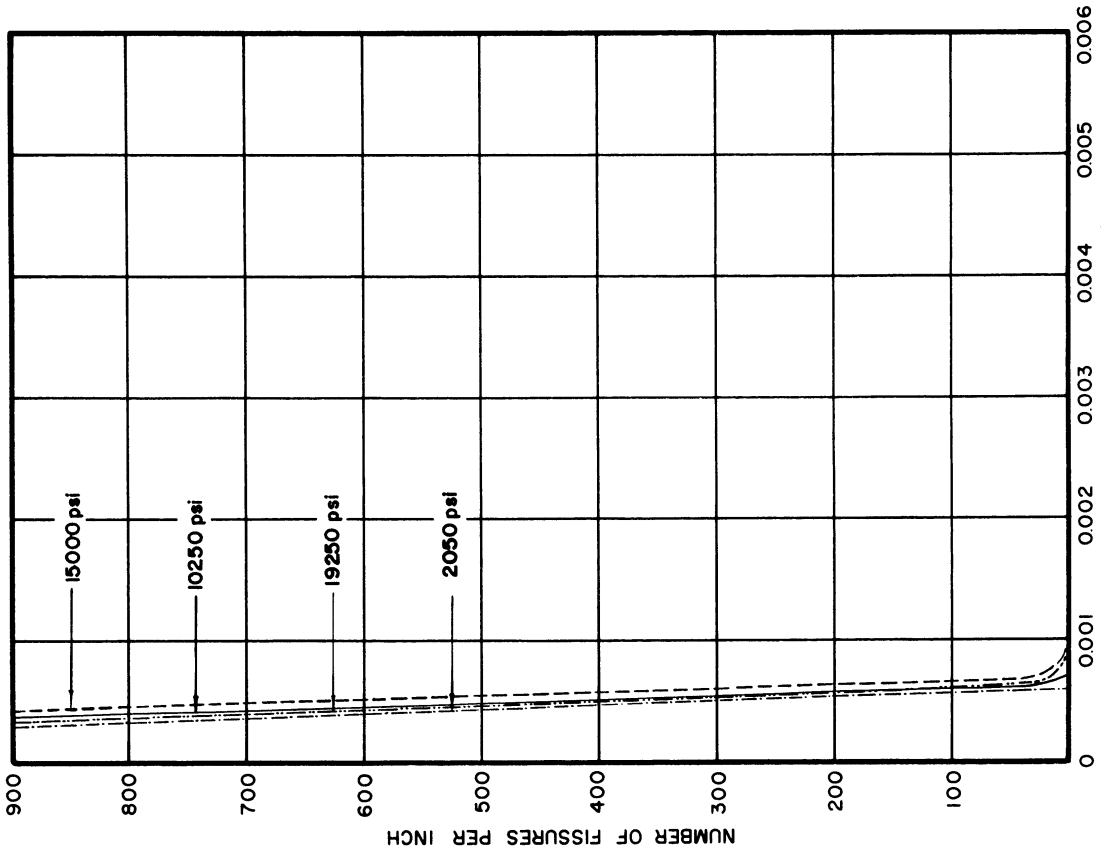

Fig. 37. Penetration vs depth below surface. Hastelloy B, heat B-1400. 1200°F, 100 hours.

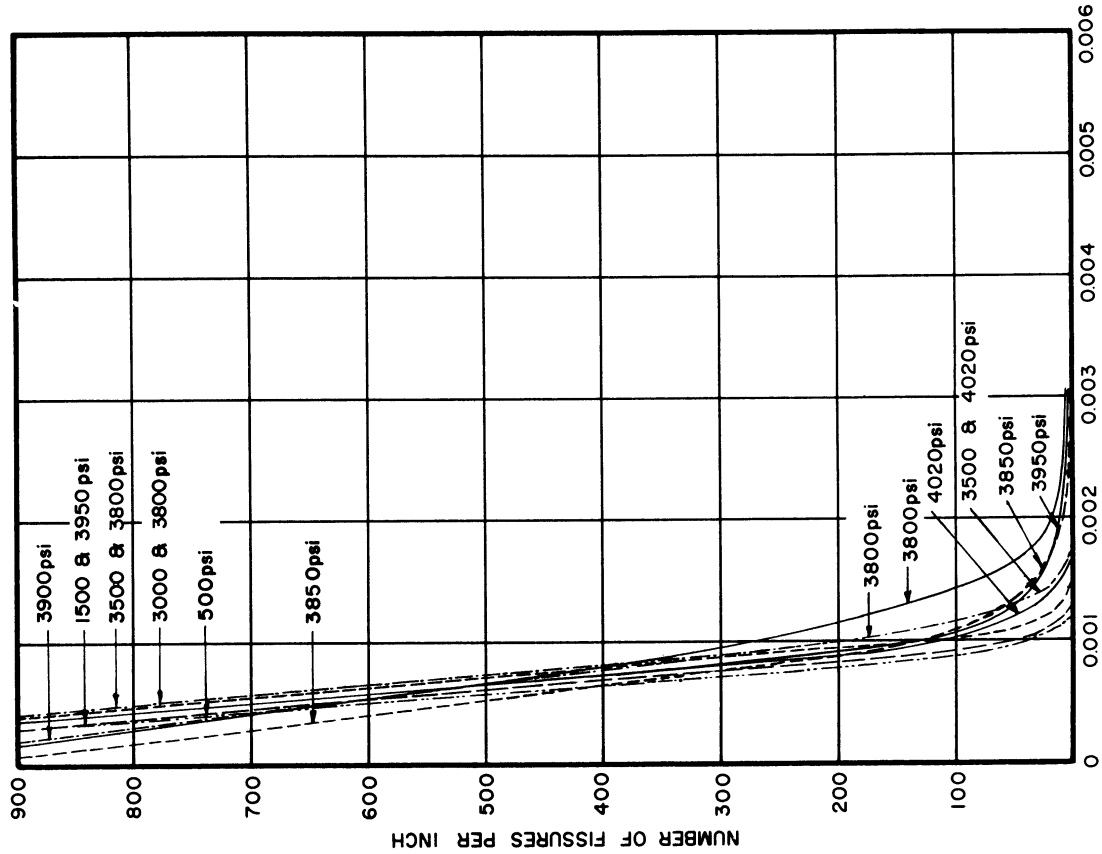

Fig. 40. Penetration vs depth below surface. Hastelloy B, heat B-1400. 1800°F, 100 hours.

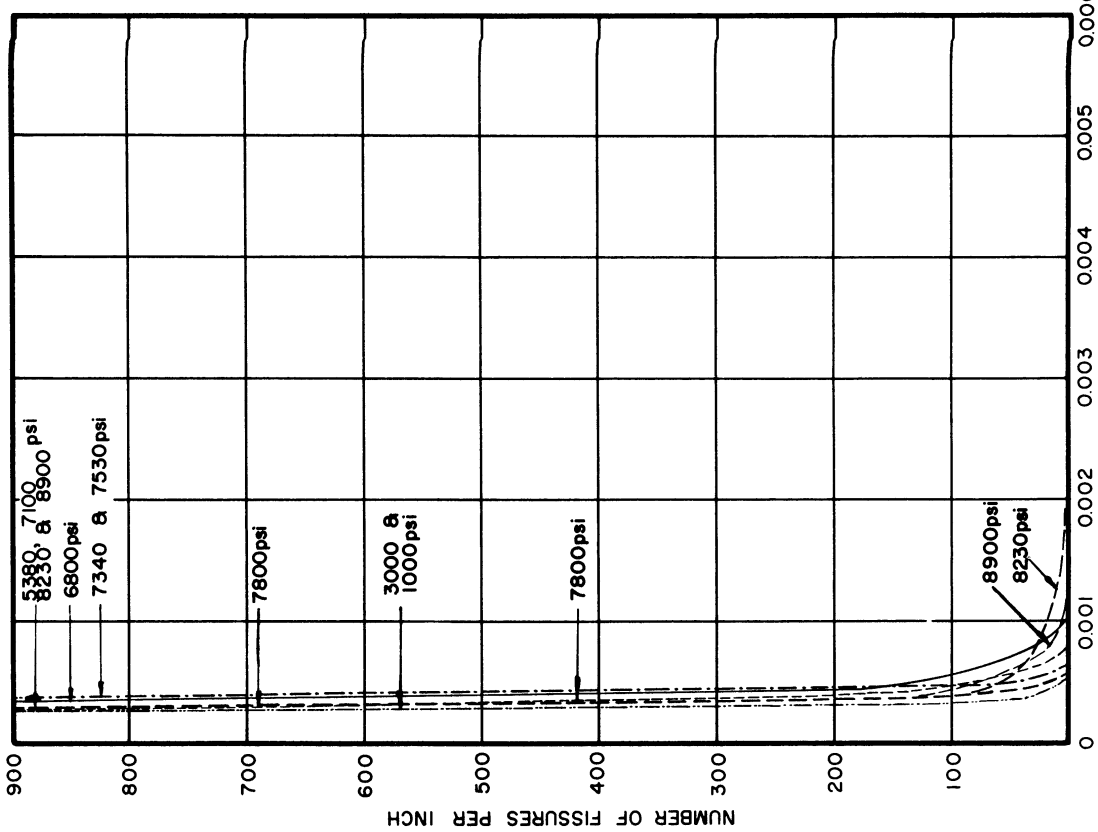

Fig. 39. Penetration vs depth below surface. Hastelloy B, heat B-1400. 1600°F, 100 hours.

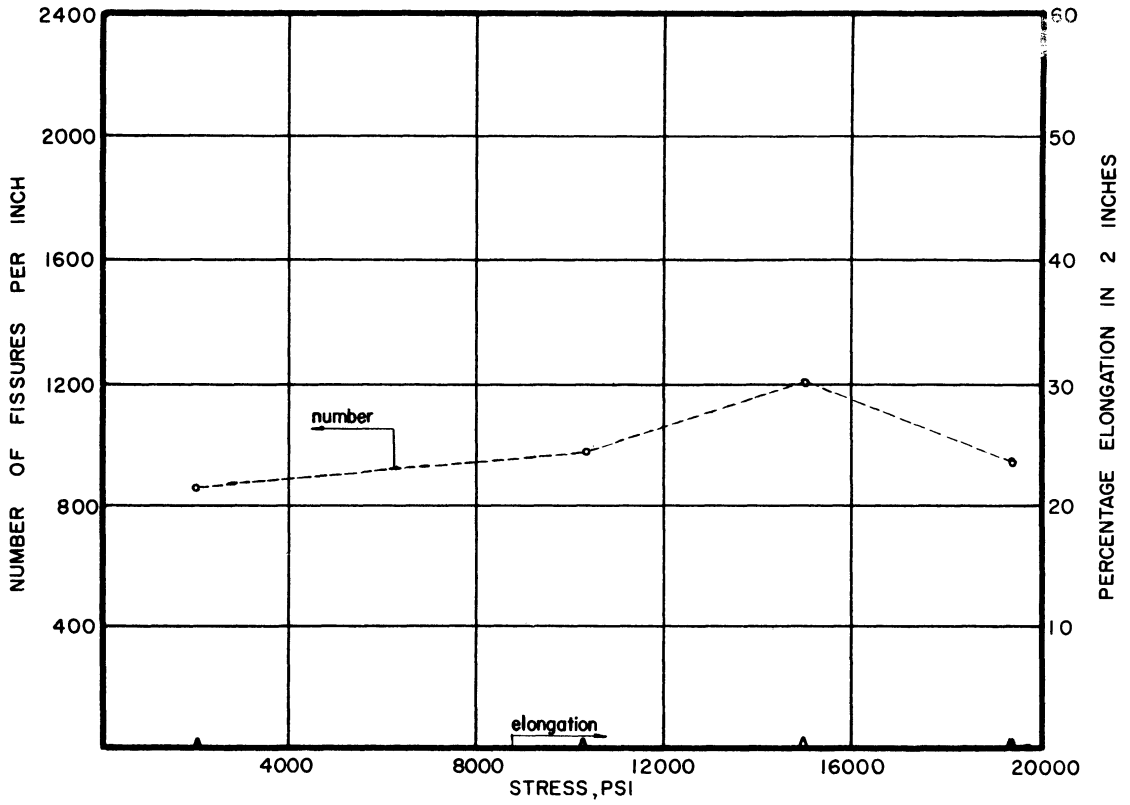

Fig. 41. Summary penetration-frequency curves.
Hastelloy B, heat B-1400. 1200°F, 100 hours.

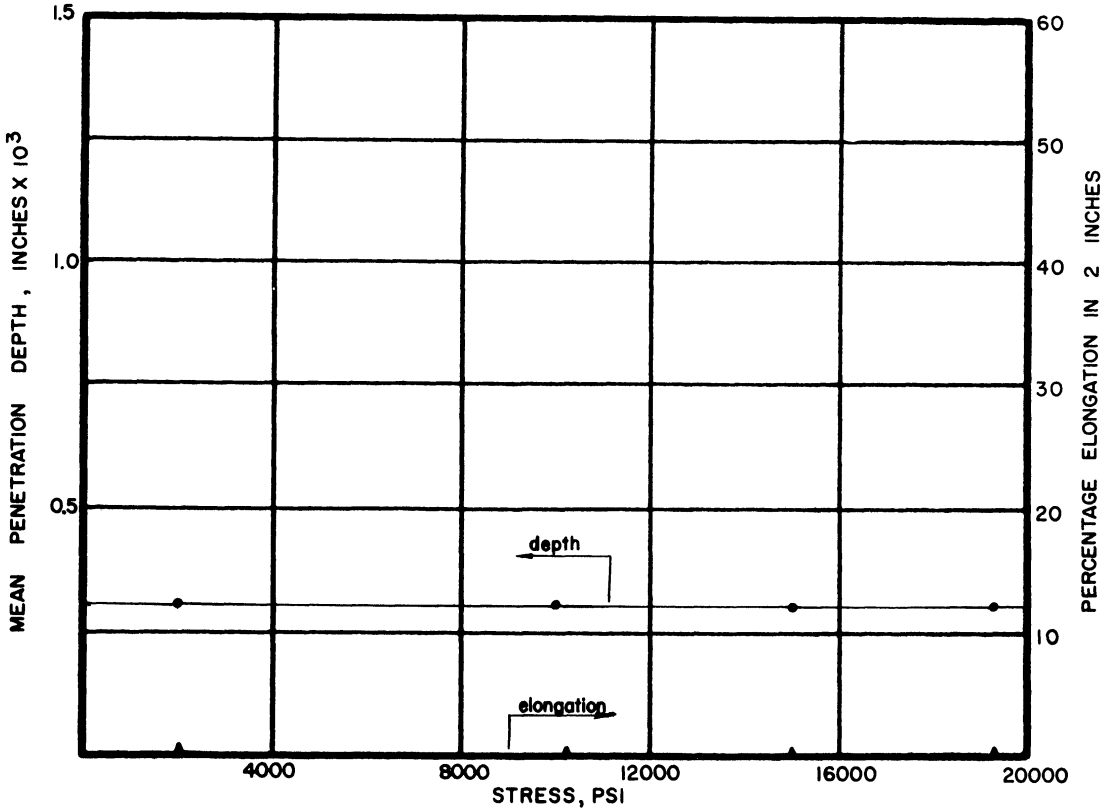

Fig. 42. Summary penetration-depth curves.
Hastelloy B, heat B-1400. 1200°F, 100 hours.

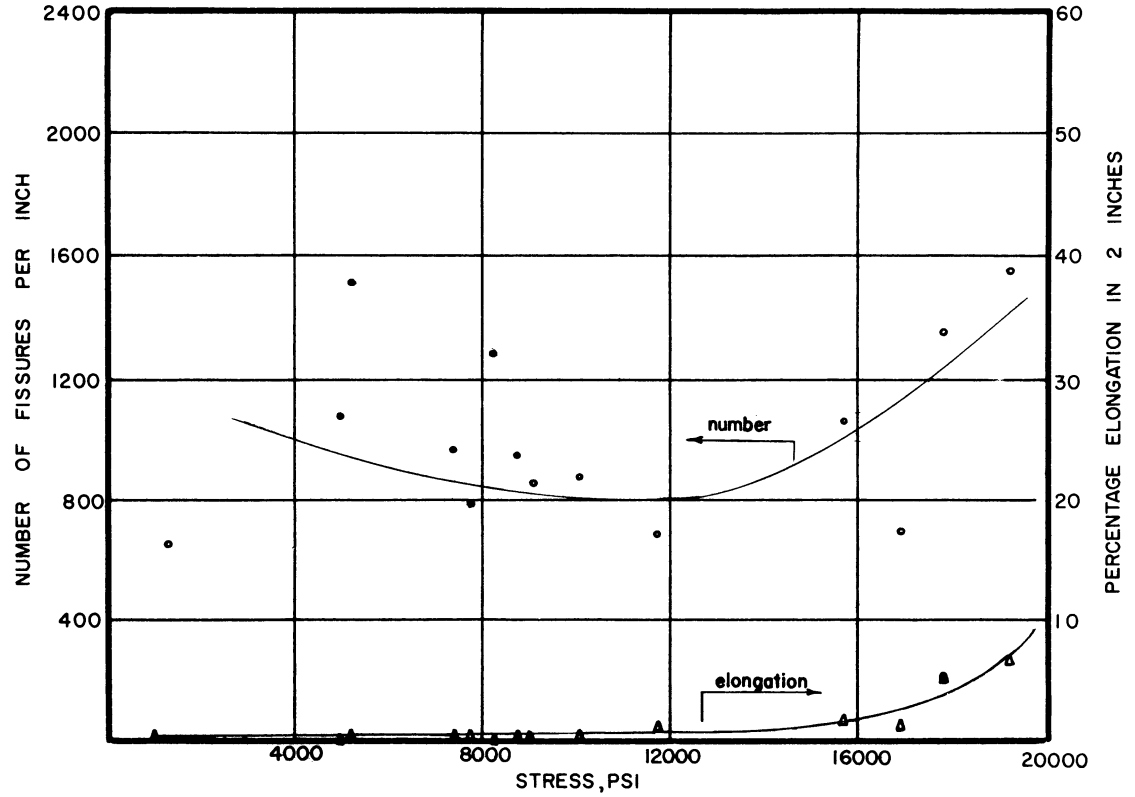

Fig. 43. Summary penetration-frequency curves.
Hastelloy B, heat B-1400. 1400°F, 100 hours.

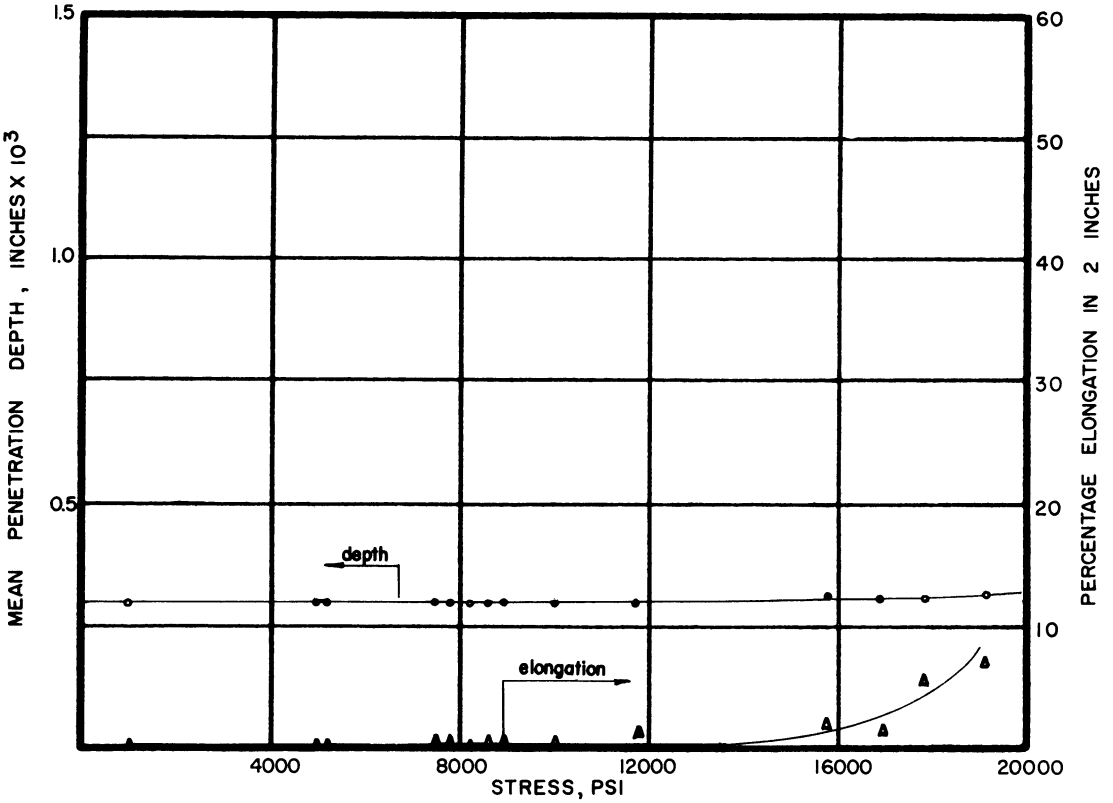

Fig. 44. Summary penetration-depth curves.
Hastelloy B, heat B-1400. 1400°F, 100 hours.

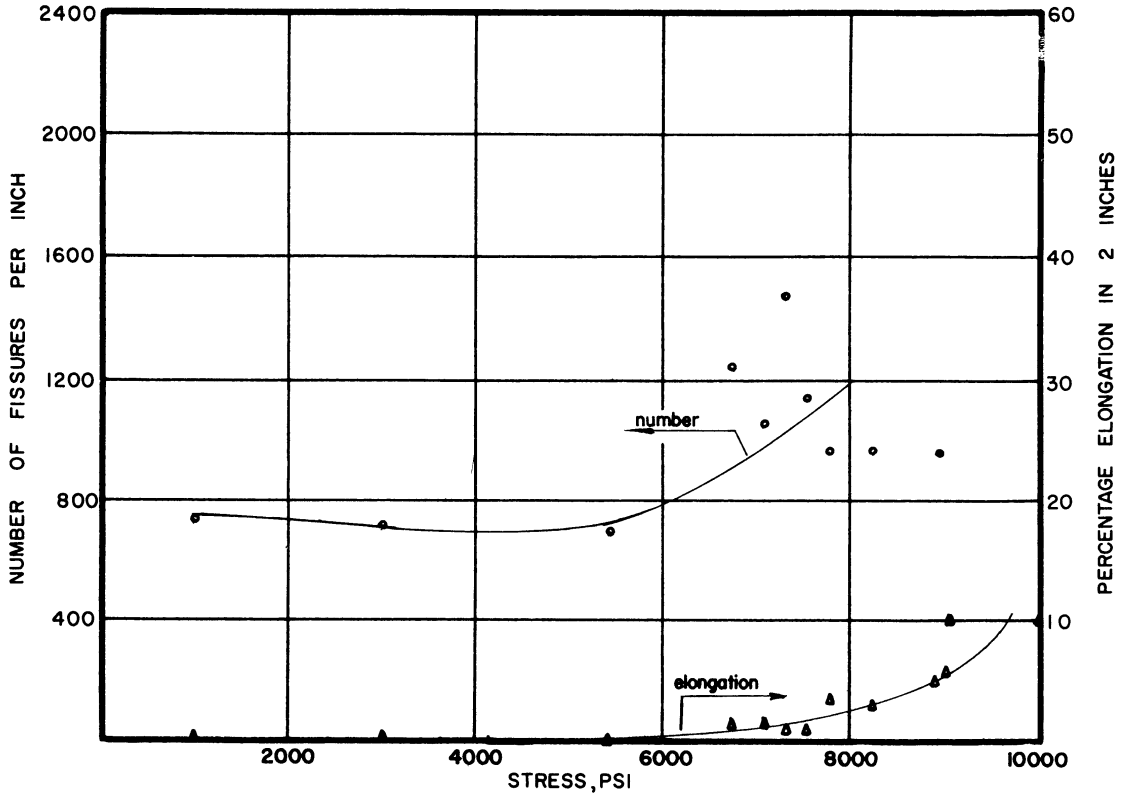

Fig. 45. Summary penetration-frequency curves.
Hastelloy B, heat B-1400. 1600°F, 100 hours.

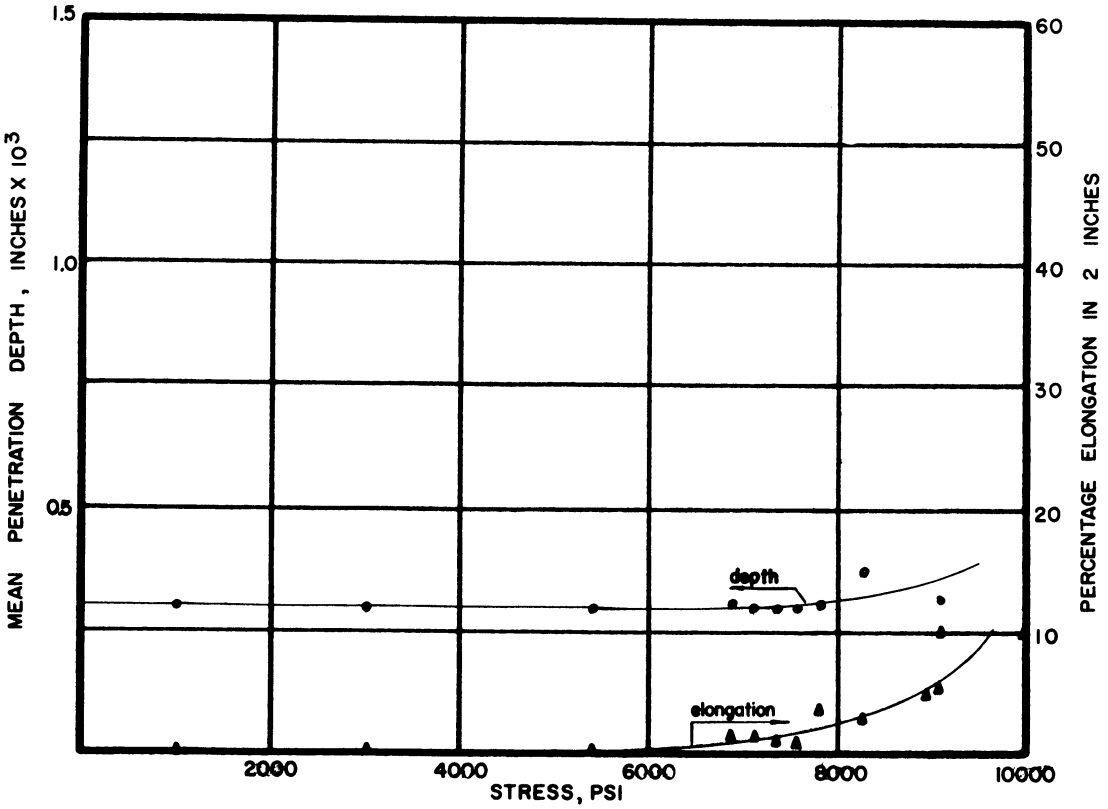

Fig. 46. Summary penetration-depth curves.
Hastelloy B, heat B-1400. 1600°F, 100 hours.

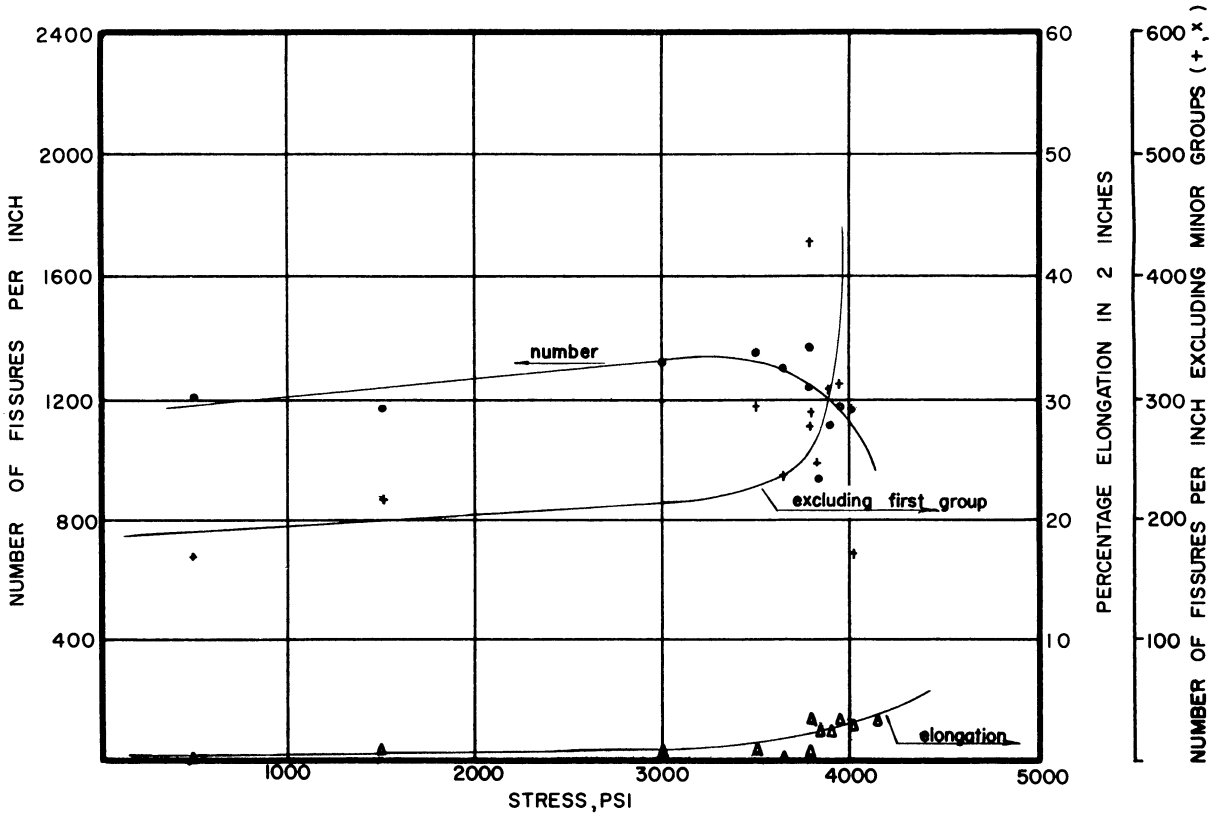

Fig. 47. Summary penetration-frequency curves.
Hastelloy B, heat B-1400. 1800°F, 100 hours.

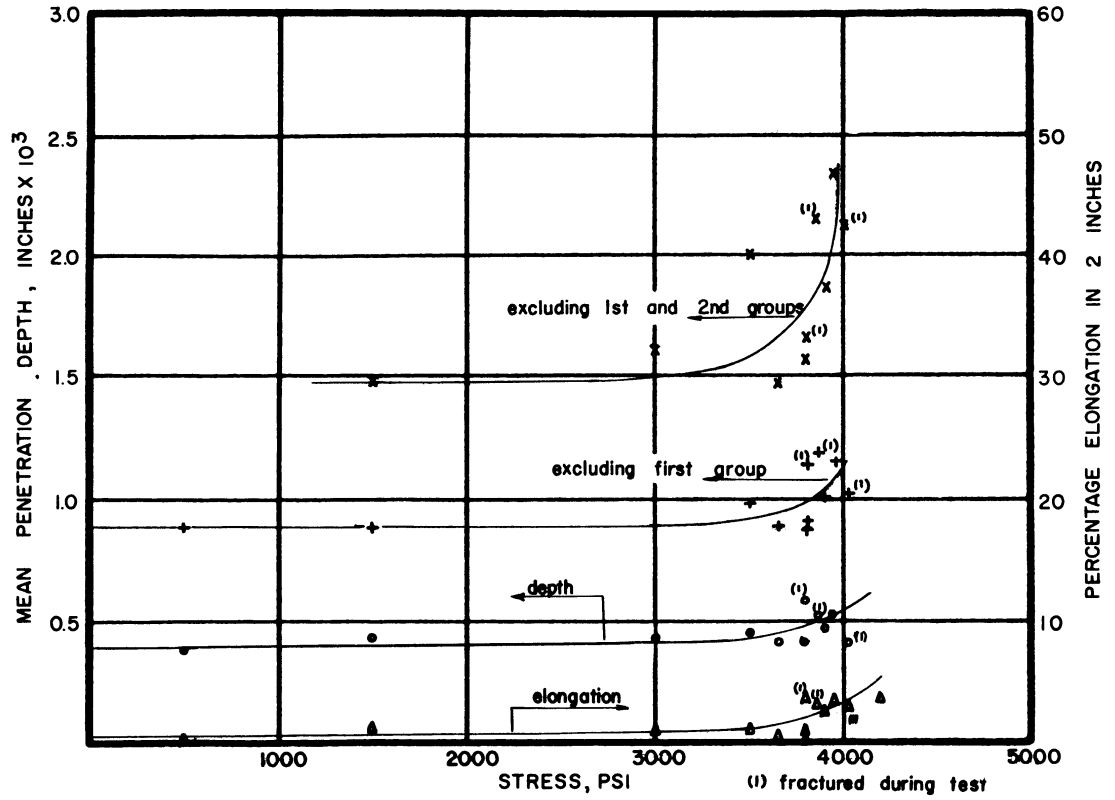

Fig. 48. Summary penetration-depth curves.
Hastelloy B, heat B-1400. 1800°F, 100 hours.

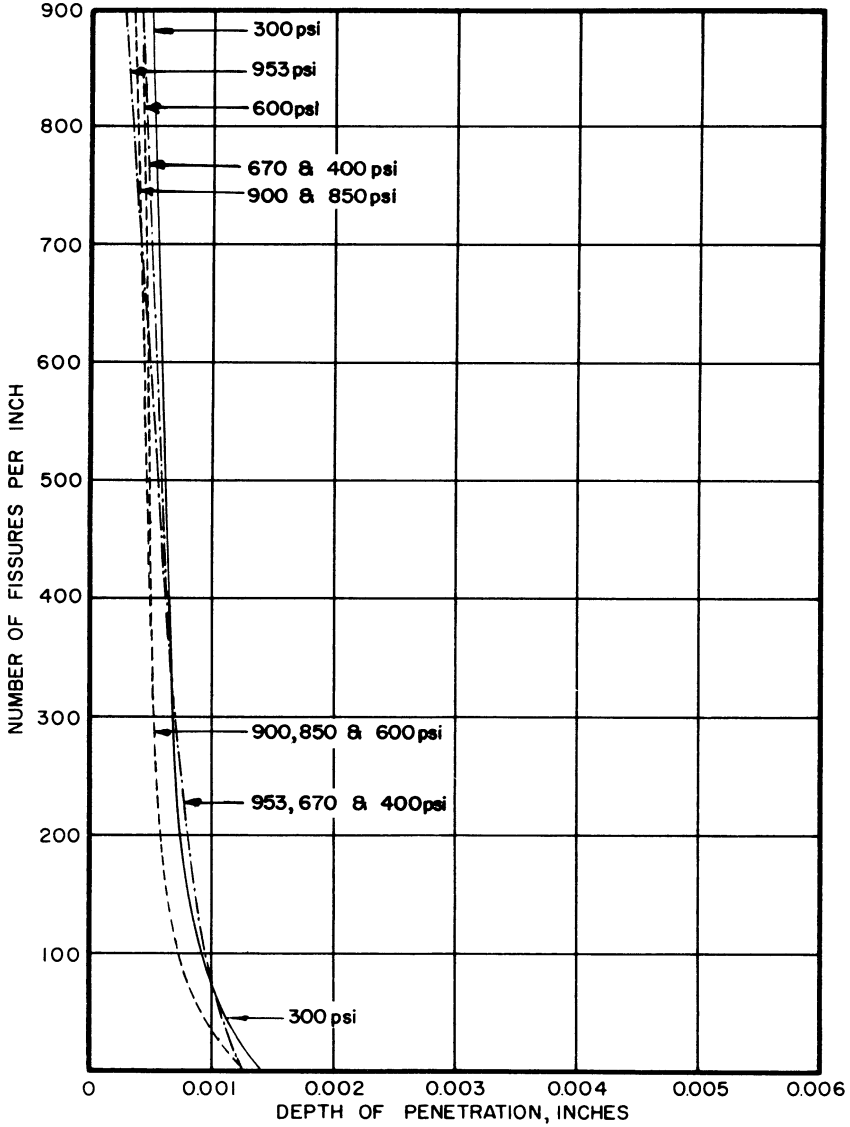

Fig. 49. Penetration vs depth below surface. Type 310 alloy, heat 4X-343. 1900°F, 100 hours.

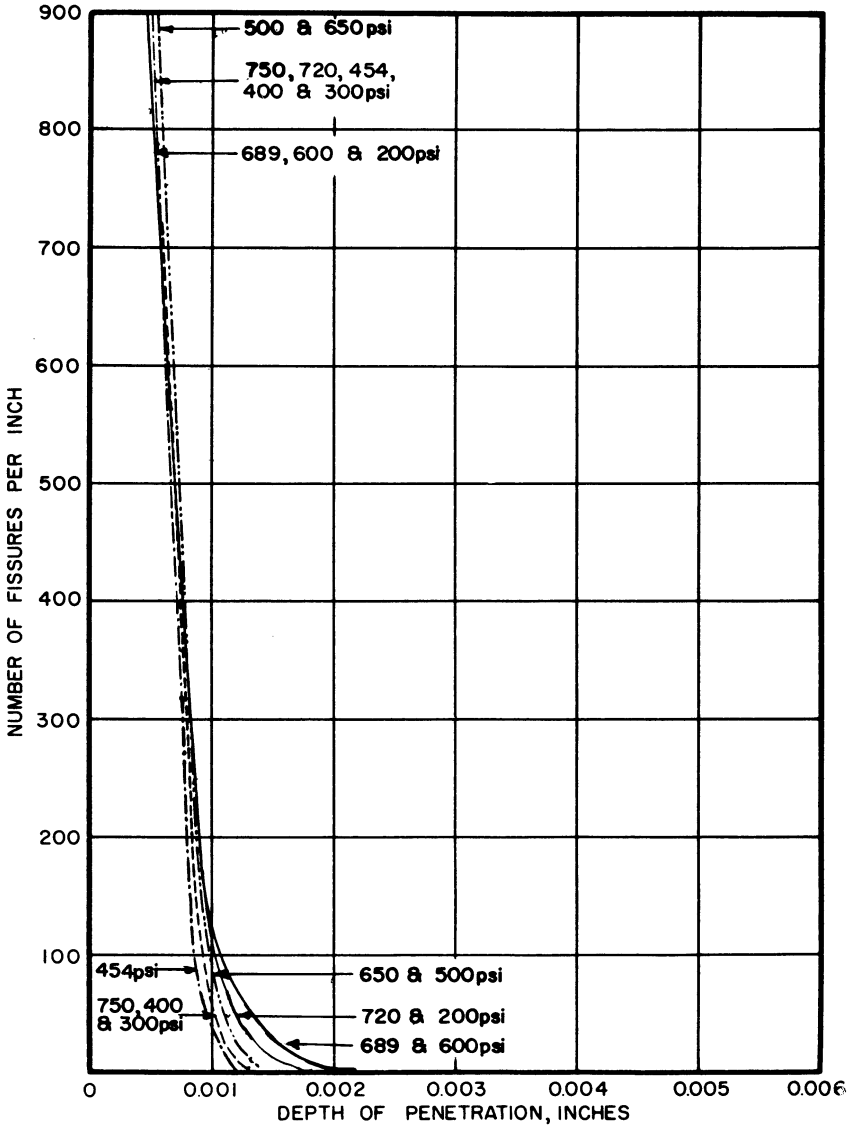

Fig. 50. Penetration vs depth below surface. Type 310 alloy, heat 4X-343. 2000°F, 100 hours.

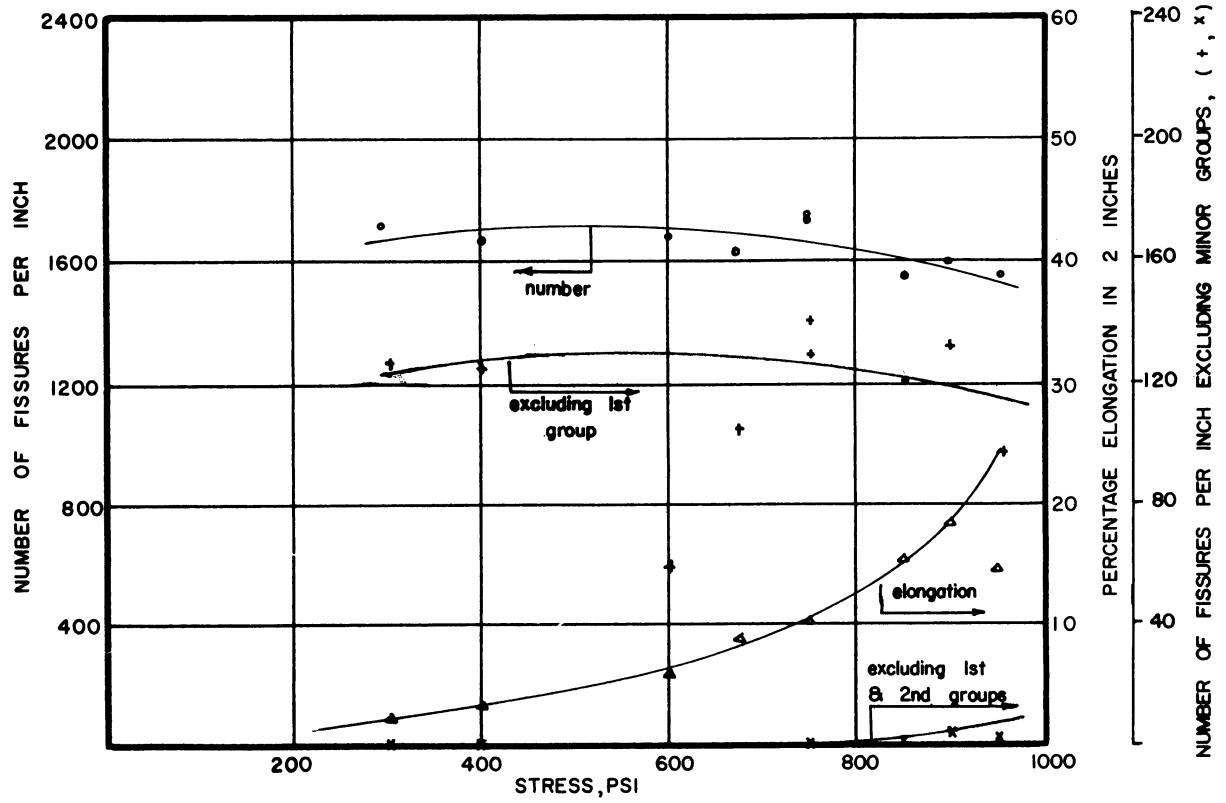

Fig. 51. Summary penetration-frequency curves.
Type 310 alloy, heat 4X-343. 1900°F, 100 hours.

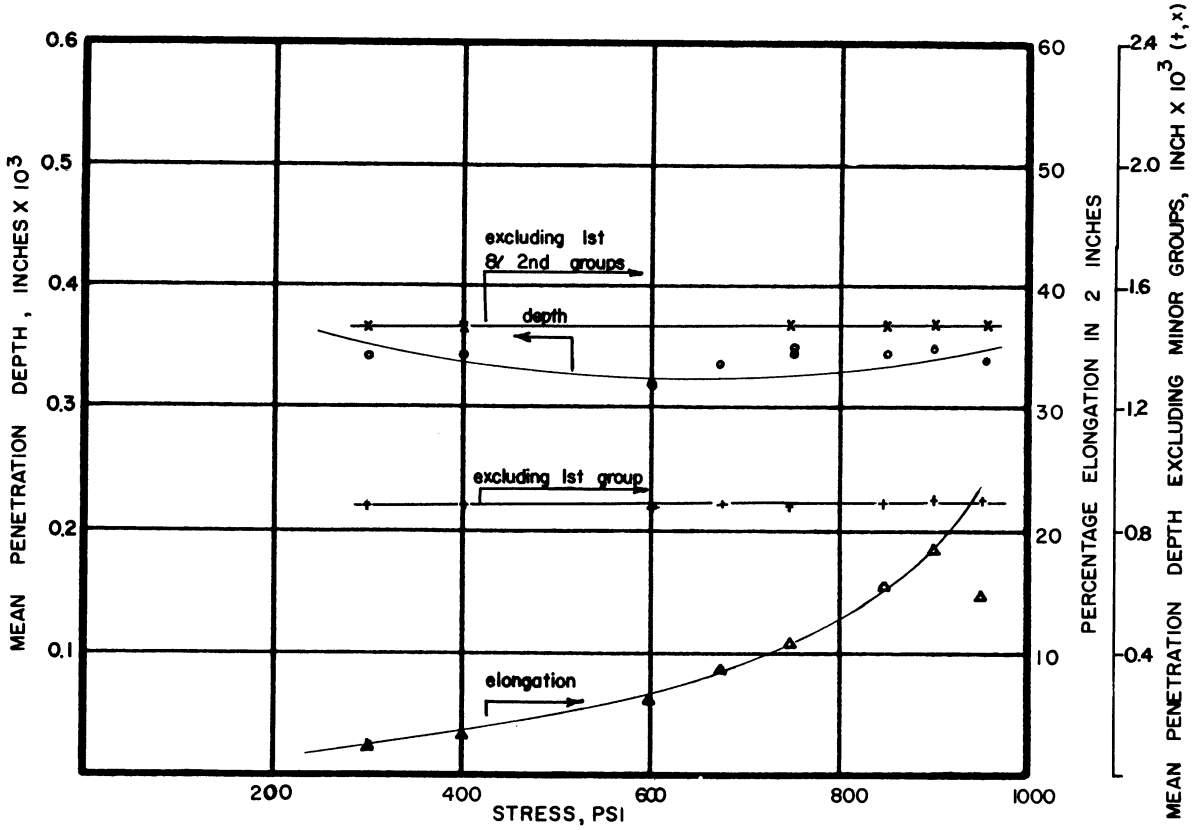

Fig. 52. Summary penetration-depth curves.
Type 310 alloy, heat 4X-343. 1900°F, 100 hours.

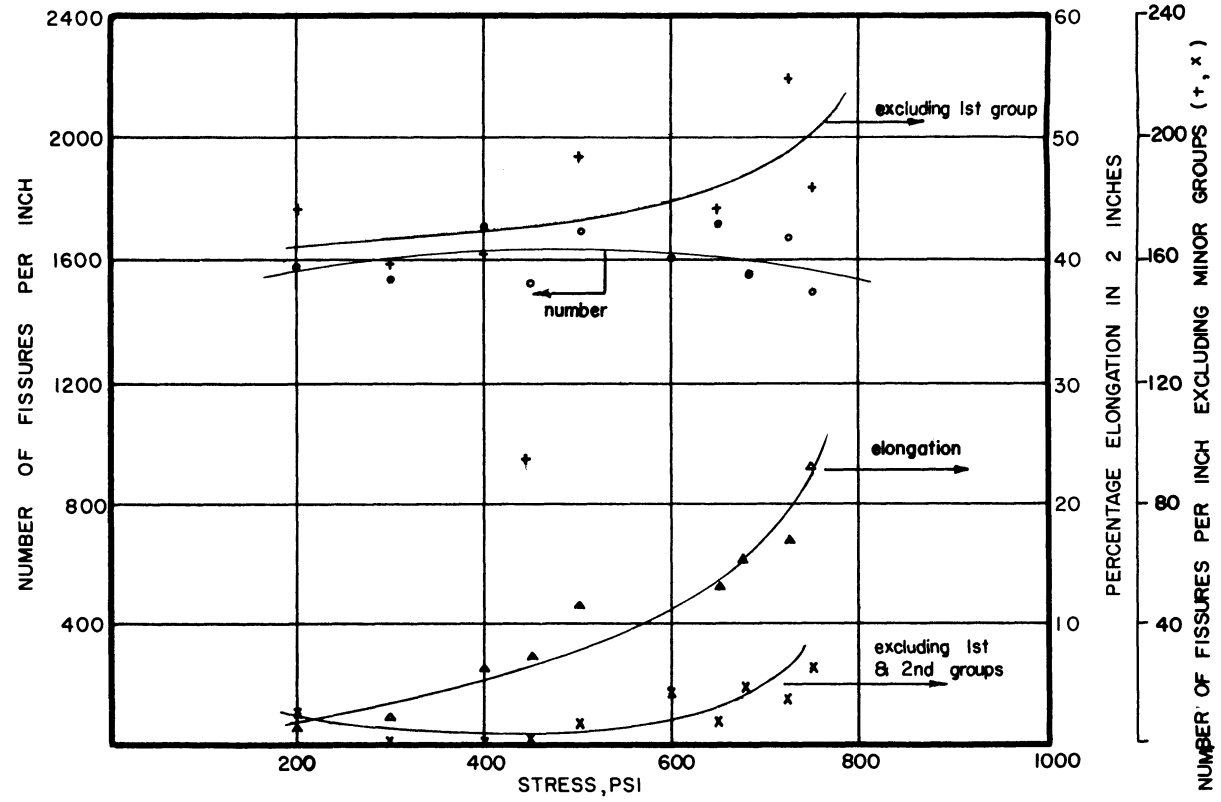

Fig. 53. Summary penetration-frequency curves.
Type 310 alloy, heat 4X-343. 2000°F, 100 hours.

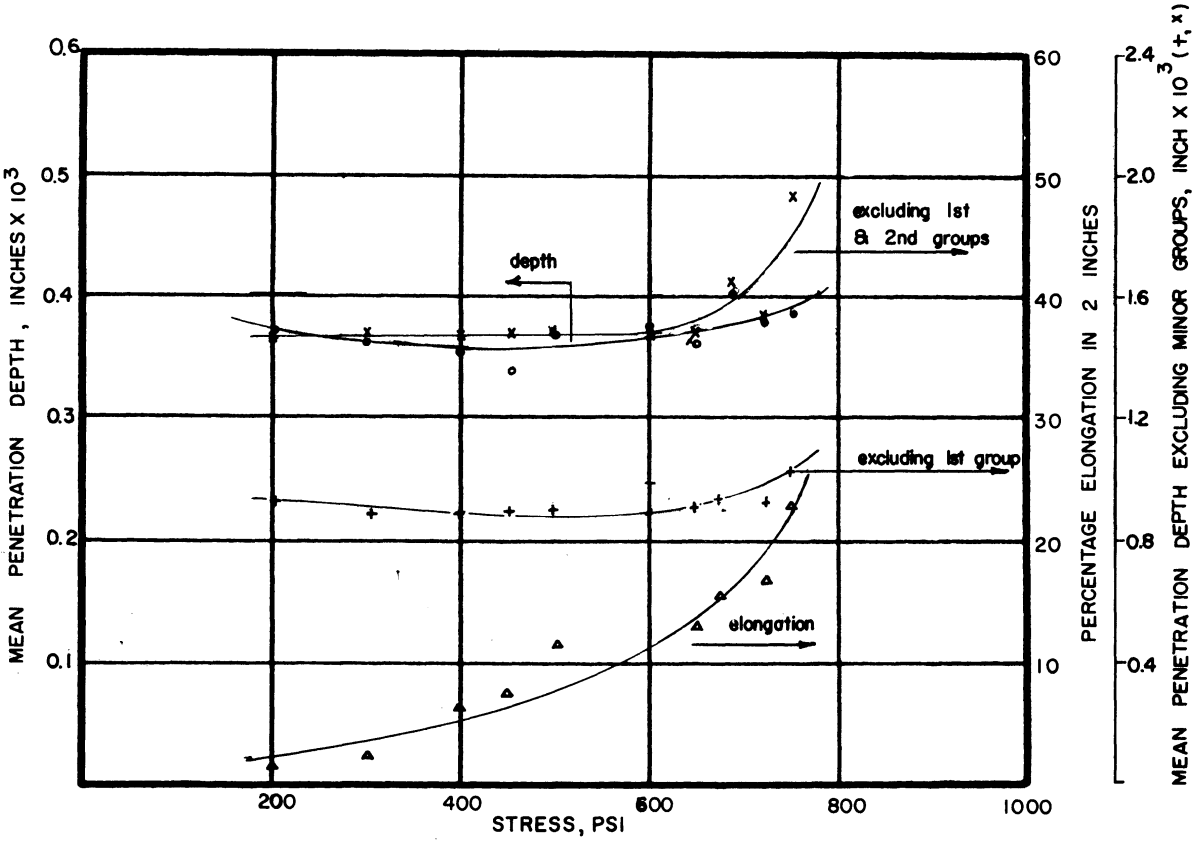

Fig. 54. Summary penetration-depth curves.
Type 310 alloy, heat 4X-343. 2000°F, 100 hours.

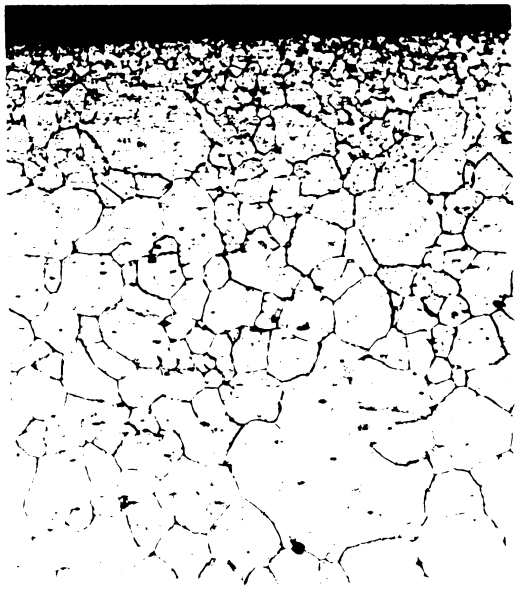

Fig. 55. Chromel alloy ASM, as received. 250x; cross section, etched electrolytically in 1-1-5 HCl, HNO_3, H_2O solution.

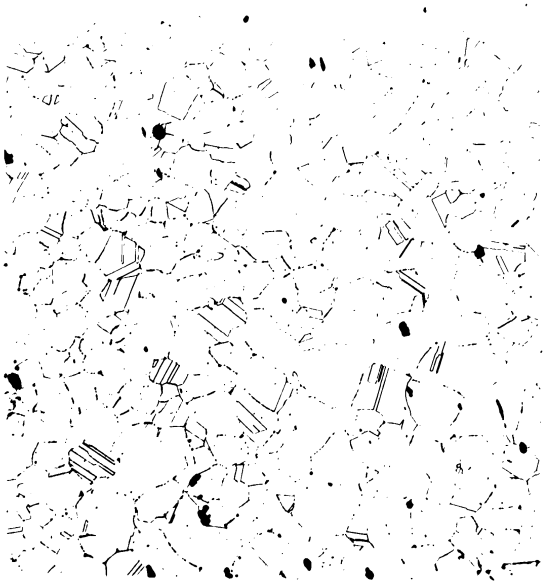

Fig. 56. Type 310 alloy, heat 25139. As received. 100x; cross section, etched electrolytically in chromic acid.

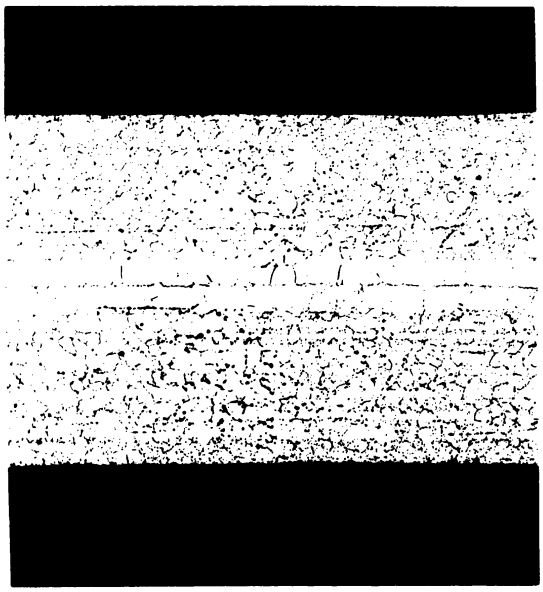

Fig. 57. Hastelloy B alloy, heat B-1400. 50x; cross section, etched electrolytically in chromic acid.

Fig. 58. Type 310 alloy, heat 4X-343. As received. 100x; cross section, etched electrolytically in chromic acid.

Fig. 59. Type 310 alloy, heat 25139. 1700°F, 100 hours, stress 2245 psi. 100x; cross section, etched electrolytically in oxalic acid.

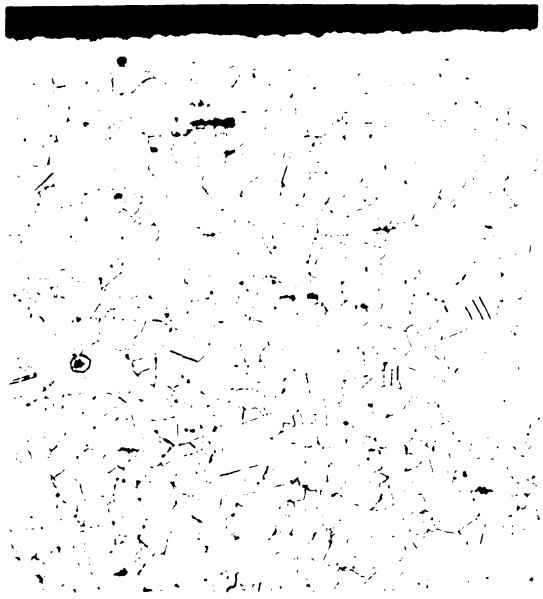

Fig. 60. Type 310 alloy, heat 25139. 1800°F, 100 hours, stress 1580 psi. 100x; cross section, etched electrolytically in oxalic acid.

Fig. 61. Type 310 alloy, heat 25139. 1900°F, 100 hours, stress 755 psi. 100x; cross section, etched electrolytically in oxalic acid.

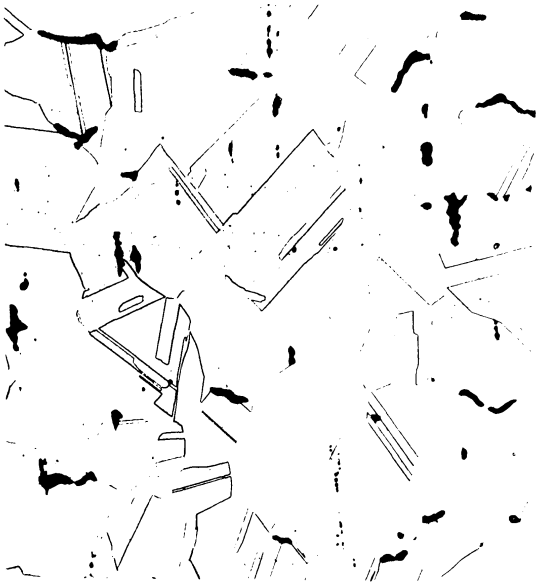

Fig. 62. Type 310 alloy, heat 25139. 2000°F, 100 hours, stress 755 psi. 100x; cross section, etched electrolytically in oxalic acid.

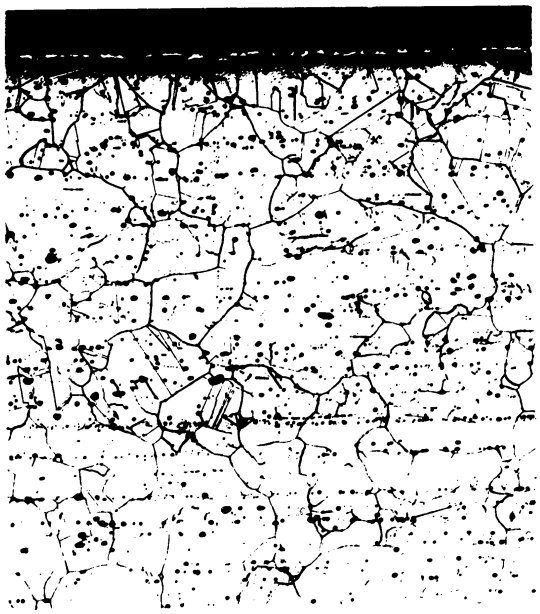

Fig. 63. Hastelloy B, heat B-1400. 1200°F, 100 hours, stress 19,250 psi. 100x; cross section, etched electrolytically in chromic acid.

Fig. 64. Hastelloy B, heat B-1400. 1400°F, 100 hours, stress 10,000 psi. 75x; cross section, etched electrolytically in chromic acid.

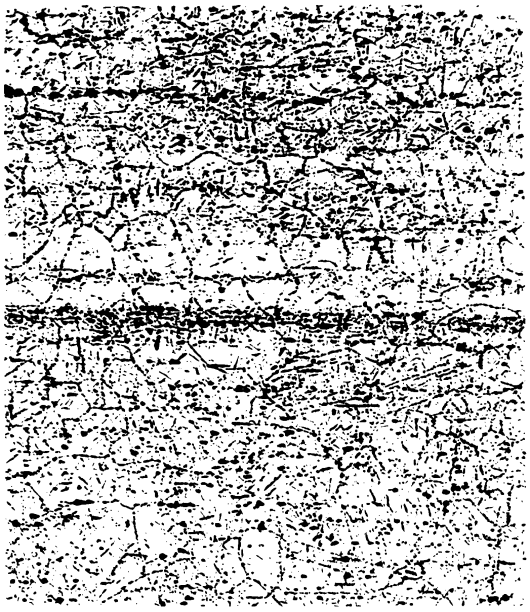

Fig. 65. Hastelloy B, heat B-1400. 1600°F, 100 hours, stress 7800 psi. 100x; cross section, etched electrolytically in chromic acid.

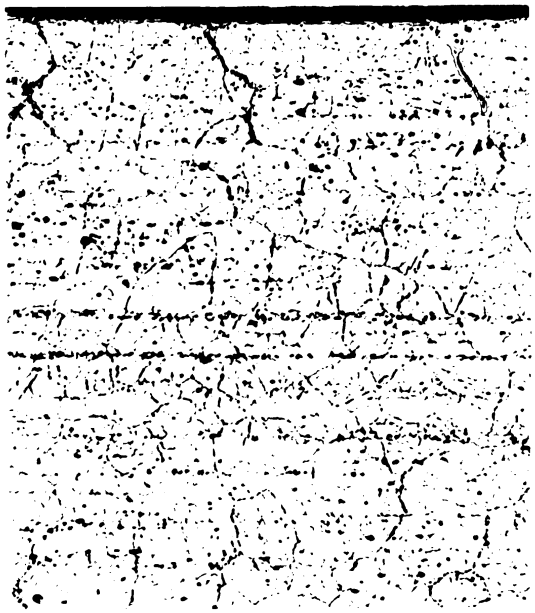

Fig. 66. Hastelloy B, heat B-1400. 1800°F, 100 hours, stress 4180 psi. 100x; cross section, etched electrolytically in chromic acid.

Fig. 67. Type 310 alloy, heat 4X-343. 1900°F, 100 hours, stress 750 psi. 100x; cross section, etched electrolytically in chromic acid.

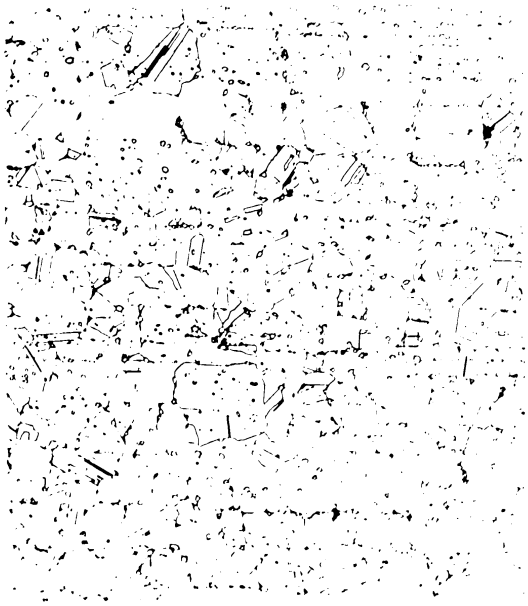

Fig. 68. Type 310 alloy, heat 4X-343. 2000°F, 100 hours, stress 600 psi. 100x; cross section, etched electrolytically in oxalic acid.

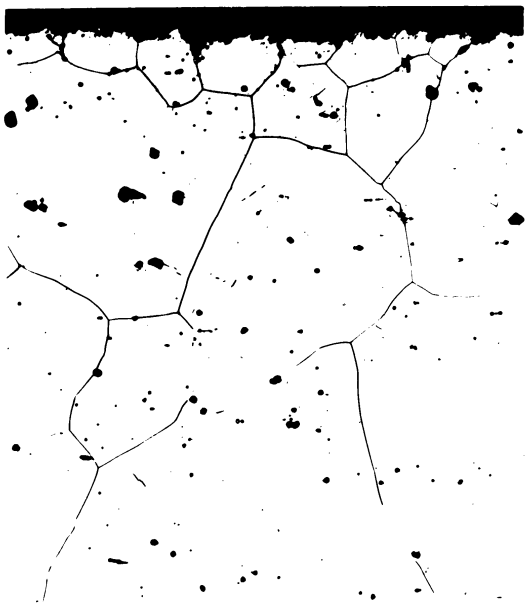

Fig. 69. Chromel ASM alloy, 2000°F, 100 hours, stress 750 psi. 250x; cross section, etched electrolytically in 1-1-5 HCl, HNO_3, H_2O solution.

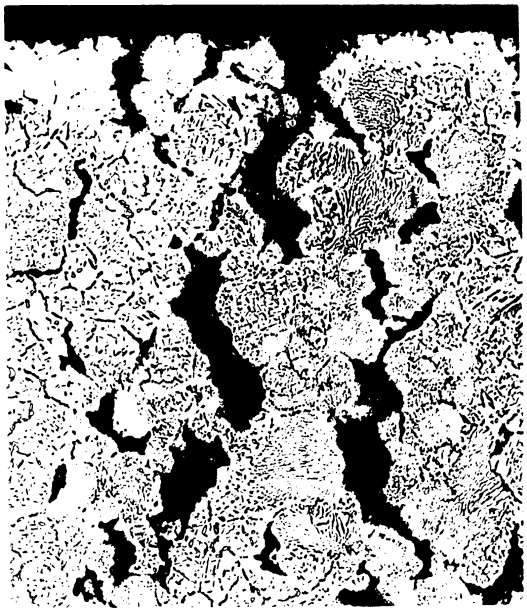

Fig. 70. Type 310 alloy, heat 25139. 1900°F, 100 hours, stress 1096 psi. 100x; cross section, unetched.